Climate Dynamics (2019) 52:6279–6300
https://doi.org/10.1007/s00382-018-4511-x

The El Niño–Southern Oscillation's effect on summer heatwave development mechanisms in Australia

Tammas Francis Loughran[1,2] · **Andrew J. Pitman**[1,3] · **Sarah E. Perkins-Kirkpatrick**[1,2]

Received: 20 September 2017 / Accepted: 19 October 2018 / Published online: 10 November 2018

Abstract
We investigate how the El Niño–Southern Oscillation (ENSO) affects the mechanisms and development of heatwaves in Australia. There are three fundamental mechanisms through which heat can accumulate in the atmosphere to generate temperatures high enough, and long-lasting enough to cause a heatwave. First, heat is advected, usually from lower latitudes, via a slow moving synoptic high pressure system; second, via diabatic heating of the boundary layer by the land surface; and third, via the subsidence of high potential temperature air which warms adiabatically as it approaches the heatwave affected region. Using an atmospheric model, we examine how ENSO affects these three mechanisms using prescribed sea surface temperatures characteristic of El Niño and La Niña conditions. By generating multiple ensembles of the same ENSO conditions, we can generate many ENSO realisations and examine how this large-scale mode of variability influences Australian heatwaves. We find that heatwave frequency and duration in the north and northeast are primarily affected by ENSO through land surface processes, soil moisture and changes in the surface energy balance. The importance of atmosphere–land coupling in ENSO related heatwave variability may help explain El Niño events with unusually few heatwaves and improve seasonal heatwave predictions. Other heatwave development mechanisms, such as the advection of heat and the subsidence of adiabatically warming air, are more important for the southern regions of Australia, but the influence of ENSO is weaker. The southeast tends to receive little influence from ENSO.

Keywords Heatwaves · El Niño · Variability

1 Introduction

Heatwaves are prolonged periods of extreme heat lasting at least three consecutive days (Perkins and Alexander 2013). They have the highest mortality rate of any natural disaster in Australia (Coates 1996) and cause substantial labour productivity losses (Zander et al. 2015). For example, in the most recent assessment of the economic burden of heat stress, Zander et al. (2015) showed existing risks associated with extreme heat represented an annual economic burden of around US$6.2 billion (0.33–0.47% of Australia's GDP) for the Australian workforce. They can adversely impact agriculture by decreasing crop yield (Decker 1967; Farooq et al. 2016) and impact other sensitive ecosystems (e.g. Welbergen et al. 2008). Heatwaves affect human mortality and over 370 deaths were linked to the heatwave preceding the Black Saturday bushfires in 2009 (Victorian Department of Health 2009; Coates et al. 2014). Globally, heatwaves accounted for 148,000 of the 164,000 lives lost due to extreme temperatures and 92% of heatwave deaths occurred in high-income countries (CRED 2015). They have also caused infrastructure failures (McEvoy et al. 2012) and stress power supply (Colombo et al. 1999).

Since 1950, the intensity, frequency and duration of heatwaves have increased globally (Frich et al. 2002; Perkins et al. 2012) and over Australia (Perkins and Alexander 2013) at an accelerating rate in recent decades (Coumou and Rahmstorf 2012). Most recently, in 2016, Melbourne, Adelaide and Sydney all experienced record high day and night temperatures (Bureau of Meteorology 2016b).

✉ Tammas Francis Loughran
t.loughran@lmu.de

[1] Climate Change Research Centre, Faculty of Science, University of New South Wales, Level 4, Mathews Building, Sydney, NSW 2052, Australia

[2] Australian Research Council Centre of Excellence for Climate System Science, Sydney, Australia

[3] Australian Research Council Centre of Excellence for Climate Extremes, Sydney, Australia

Sydney, for example, experienced 39 days in a row at or above 26 °C (Green et al. 2017).

The austral summer of 2015–2016 experienced one of the strongest El Niño events on record coincident with the warmest year on record globally (World Meteorological Organisation 2016). Australia also experienced above average temperatures (Bureau of Meteorology 2016a) and a record breaking heatwave in the southeast of the continent (Bureau of Meteorology 2016b). The El Niño–Southern Oscillation (ENSO), which consists of quasi periodic warm (El Niño) and cold (La Niña) phases of sea surface temperatures (SSTs) in the equatorial eastern Pacific, explains a large portion of the interannual variability of Australian heatwaves (Nicholls et al. 2005; Arblaster and Alexander 2012; Perkins et al. 2015; Loughran et al. 2017a). Understanding how ENSO influences the mechanisms responsible for heatwave development is important for predicting future seasonal heatwave behaviour, particularly in the context of a warming climate where hotter, longer and more frequent heatwaves are projected (Meehl and Tebaldi 2004; Cowan et al. 2014).

The three fundamental mechanisms of how heat accumulates in the atmosphere preceding and during Australian heatwave events are summarised by McBride et al. (2009). These mechanisms are: advection from lower latitudes; large-scale subsidence transporting higher potential temperature air from upper levels; and surface heating involving the development of the diurnal mixed layer, and replacement from below by the new mixed layer of the successive days.

The first mechanism refers to horizontal advection of heat from other regions, usually lower latitudes or hot and dry interiors of continental regions, driven by a slow moving anticyclone to the east of the heatwave affected area. The synoptic structure of anticyclones associated with southeast Australian heatwaves are well described as part of a baroclinic Rossby wave train that develops over the Indian Ocean and breaks near the Tasman Sea (Pezza et al. 2012). The sea level high pressure system is also associated with upper level anticyclonic potential vorticity that is advected into the region, and which also sustains the persistence of the anticyclone (Parker et al. 2014a). While the anticyclone is sometimes identified in these studies as a blocking high, Marshall et al. (2013) made the important distinction for the Australian case that they are in fact "persistent highs". Persistent highs are located at a distinctly lower latitude than blocking highs, and do not feature a split in the polar jet stream. The difference in the synoptic patterns for each ENSO phase was explored for southeastern Australia by Parker et al. (2014b) who showed that despite the anticyclone being stronger during El Niño, Victorian heatwaves are more frequent during La Niña when the northerly air circulation and upper level potential vorticity anomalies are stronger. However the influence that ENSO has on the synoptic patterns for heatwaves in other regions of Australia has not been fully explored.

The second mechanism enabling heat to accumulate during a heatwave relates to vertical movement of air that is warmed adiabatically. For heatwaves in southeastern Australia, air tends to originate at high altitudes from the westerlies over the Southern Ocean, circulate around a high pressure system over the Tasman Sea, and descend to finally approach the heatwave affected region from the north (McBride et al. 2009; Boschat et al. 2014). As air descends it is warmed adiabatically. Over Europe, Bieli et al. (2015) used a Lagrangian approach to evaluate changes in potential temperature preceding hot extremes, and found that the adiabatic warming and diabatic heating contribution to temperature for air parcels that approach hot extremes can vary regionally. This approach has recently been applied to the state of Victoria in southeastern Australia by Quinting and Reeder (2017), who examined the origins of air masses and the sources of potential vorticity that sustains the anticyclone associated with heatwaves in the region. They identified a number of sources of potential heat and vorticity. For example, the temperature of air parcels approaching heatwave locations is raised equally strongly by adiabatic warming and diabatic heating processes. However, the exact role of the subsidence of potential heat from aloft during each ENSO phase is still unknown for any region of Australia.

The third heat accumulation mechanism relates to the diabatic heating of air leading up to and during a heatwave via land surface heating and associated feedbacks. During conditions of high soil moisture, turbulent energy transferred to the atmosphere from the land surface is predominantly in the form of latent heat via evaporation. Higher latent heating necessarily leads to less sensible heating due to energy balance constraints. On the other hand, dry soil conditions results in the surface energy balance favouring sensible heat fluxes, leading to a warmer and commonly drier atmosphere (Alexander 2011). A warmer and drier atmosphere tends to further desiccate the soil leading to a soil moisture-temperature feedback (Seneviratne et al. 2010; Miralles et al. 2012). As the surface energy balance tends towards higher sensible heating and lower latent heat fluxes, a progressive accumulation of heat can develop within the atmospheric boundary layer, increasing the potential for extreme temperature and increasing heatwave duration (Hirschi et al. 2010; Lorenz et al. 2010; Miralles et al. 2014). For Australia, soil moisture plays an essential role in heatwave development, but is ultimately insufficient on its own (Herold et al. 2016). This is particularly relevant to the north and eastern regions where ENSO has a dominating influence on precipitation and hence soil moisture. Several other studies have examined the importance of ENSO on Australian rainfall variability in station observations, reanalysis and climate models (e.g.

Nicholls et al. 1997; Risbey et al. 2009; Klingaman et al. 2013; Ashcroft et al. 2014; King et al. 2015). While the link between rainfall, ENSO and heatwaves is well-known (Perkins et al. 2015), it is by no means consistent. For example, the 1997–1998 El Niño was one of the strongest on record but had only weak impacts in Australia (Lim and Hendon 2015).

While some basic mechanisms have been identified, and the Australian heatwave–ENSO relationship has been described and quantified, an understanding of how these three mechanisms relate to ENSO spatially across Australia is lacking. The aim of this study is to identify the effects of ENSO on the three heat accumulation mechanisms outlined above, and thereby contribute to the explanation of how ENSO can modulate heatwave development.

2 Methods

2.1 Definition of heatwaves

We identify heatwaves following Nairn et al. (2009) using the Excess Heat Factor (EHF) index, which is a heat measure based on a relative threshold. The EHF has two components, one compares a three day average of daily mean temperature to the previous 30 days average, and the other compares the 3 days average to a relative threshold. The relative threshold used here is the day-of-year 90th percentile. A heatwave occurs if the EHF index is greater than 0 for at least 3 days. Since ENSO typically peaks in December, analysis was restricted to the extended austral summer period from November–March, which is when heatwaves are hottest and have their greatest impacts. We define the heatwave frequency as the sum of heatwave days, the duration as longest heatwave, and the amplitude as the hottest day of the hottest heatwave, all within the summer period as previously defined by Perkins and Alexander (2013).

2.2 Modelling approach

To investigate how ENSO controls Australian heatwave variability, a set of model simulations were performed using a climate model, the Australian Community Climate and Earth-System Simulator (ACCESS) v1.3. ACCESS has a horizontal grid resolution of 1.25° latitude by 1.875° longitude, and 38 vertical levels on height-based terrain-following co-ordinates. We used ACCESS in an atmosphere and land surface only mode with prescribed SSTs. ACCESS uses the UK Meteorological Office unified model (UM) (Davies et al. 2005) atmosphere coupled to the CSIRO Community Atmosphere Biosphere Land Exchange (CABLE) version 1.8 (Kowalczyk et al. 2013). CABLE describes land surface processes such as heat, water and carbon fluxes, for 13 surface types and 6 layers. CABLE has been extensively evaluated both independently (Abramowitz et al. 2008; Wang et al. 2011) and as part of major intercomparison projects (Zhang et al. 2013; Best et al. 2015). ACCESS was included in the CMIP5 experiments as part of Working Group 1 of the Intergovernmental Panel on Climate Change's 5th Assessment Report (IPCC 2013), where it has been shown its simulation are close to other models and observations (Bi et al. 2013). It has also been shown to simulate the impact of El Niño on Australian heatwave frequency reasonably well (Loughran et al. 2017b).

To undertake our experiments, we spun-up ACCESS for 50 years with constant year-2000-equivalent CO_2 concentrations, and an annually repeating seasonal climatology cycle (average of 1970–1999) derived from the Hadley Centre Sea Ice and Sea Surface Temperature (HadISST) monthly SST data set (Rayner 2003). The last 30 years of this spin-up were used as the control simulation because it features neutral ENSO conditions and no interannual SST variability. We constructed a set of 2 years ensemble simulations to sample ENSO events, instead of a single simulation with successive events. Ensembles are more independent and would not be consistently biased by existing atmospheric and land surface conditions from consecutive years. We restarted the atmosphere initial conditions from each 1st of January from the last 30 years of the control simulation to generate up to 30 ensembles per experiment group, which is a common method to sample internal variability in models (e.g. Deser et al. 2012; Arblaster et al. 2014).

The two experiment groups were forced with globally defined SSTs, featuring a single El Niño or La Niña event. The El Niño or La Niña event was derived from the HadISST monthly SST data set from 1970 to 2014 by compositing 2-year periods where the Niño 3.4 index reaches greater than 1 standard deviation (for El Niño) or less than 1 standard deviation (for La Niña) from the mean. The December–February mean of these composites are shown in Fig. 1 and demonstrate the spatial patterns (see Fig. 1a, b) and their temporal evolution (see Fig. 1c). Each event develops and decays over a 2-year period and reaches its peak in the December of the first year.

2.3 Heatwave composites

We anticipate heatwaves in various regions of Australia will be affected in different ways by ENSO and we therefore summarise results based on four regions of interest (Fig. 1d). These regions were selected based on an approximation of the observed influence of ENSO on heatwaves taken from Loughran et al. (2017a), where principal component analysis was used to identify the northern (129°E–136.5°E, 12°S–19.5°S), northeastern (139°E–146.5°E, 18°S–25.5°S), and eastern (145.5°E–153°E, 24°S–31.5°S) regions as

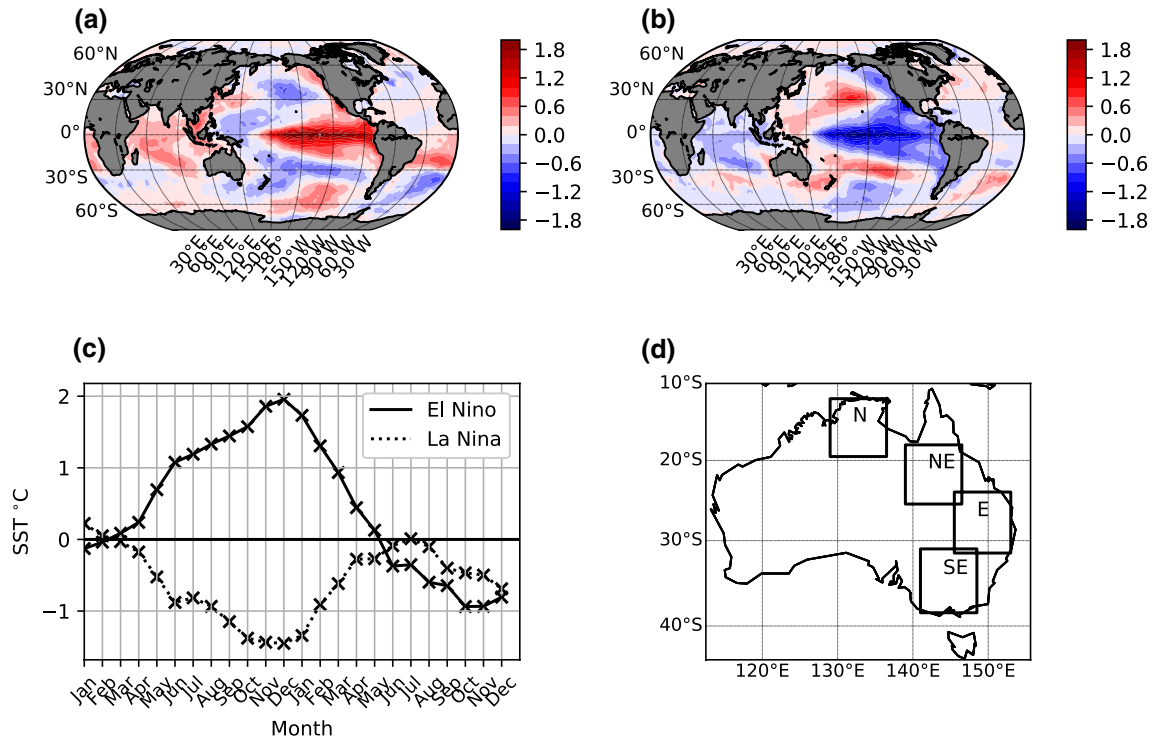

Fig. 1 DJF austral summer composite of sea surface temperature anomalies for El Niño years **a** where the Niño 3.4 index is greater than 1 standard deviation from the mean, and **b** La Niña years where Niño 3.4 index is less than 1 standard deviation. **c** Is the corresponding time series on the equator in the Pacific (93.5°W). **d** Contains the regions of interest for compositing and trajectory initiation. The regions are north (129°E–136.5°E, 12°S–19.5°S), northeast (139°E–146.5°E, 18°S–25.5°S), east (145.5°E–153°E, 24°S–31.5°S), southeast (141°E–148.5°E, 31°S–38.5°S)

being most heavily affected by ENSO. For comparison, we also included the southeast region (141°E–148.5°E, 31°S–38.5°S), where large amplitude heatwaves occur but interannual variation is either weakly or inversely related to ENSO (Boschat et al. 2014; Parker et al. 2014b).

Composites are presented for heatwaves that occur within the four regions shown in Fig. 1d. Boschat et al. (2016) give caution regarding the formulation of hypotheses based on composites, and the implications of this will be explored later in the discussion section. Heatwave days are identified when at least half of the region's area is affected by a heatwave which was done to remove single grid point exceedences of the EHF thresholds. Composites on these heatwave days were calculated for mean sea level pressure (MSLP) to ascertain changes in synoptic patterns and advection associated with ENSO. To ascertain the changes in the partitioning of net radiation associated with ENSO during heatwaves, we also composite the land surface turbulent surface sensible and latent heat fluxes (Q_H and Q_E respectively). A two-sided student's t test was used to calculate statistical significance of the composites compared to the control climatology. Values are deemed significant when there is little difference between the experiment and control groups and the null hypothesis is rejected at the 5% level.

2.4 Observational data

To compare the simulations to observations we use the NOAA Twentieth Century Reanalysis v2 (20CR) dataset (Compo et al. 2011). This reanalysis uses the NCEP Global Forecast System model, assimilated with surface pressure observations from the International Surface Pressure Databank. This reanalysis was chosen because it allows a longer analysis period compared to other reanalyses, which is required when studying interannual variability. The analysis period used for these observations is 1901–2012 which contains 17 El Niño events and 17 La Niña events. Observed heatwave days are identified based on the EHF index (as above) using daily maximum and minimum temperatures at 2 m height, and the thresholds were calculated from the 1960–2012 base-period. As above, we calculated composites of summer heatwave days for MSLP, surface latent heat flux and sensible heat flux during La Niña or El Niño. El Niño and La Niña austral summer seasons are identified as in Sect. 2.2 using Niño 3.4 index derived from HadISST SSTs.

2.5 Backward trajectory analyses

Six hourly horizontal and vertical winds from the simulations were used for calculating 10 days backward air parcel trajectories to examine the vertical and horizontal origins of air approaching heatwaves and the evolution of potential heat. The trajectories were calculated using Traj3d, a three-dimensional spherical trajectory algorithm described in detail by Noone and Simmonds (1999) and Barras and Simmonds (2009). Sub-grid scale convection and circulations are not resolved in the ACCESS winds output data, therefore the effect of small scale winds on the trajectories cannot be accounted for. Temperature (T) and hydrostatic pressure (p) were tracked along the trajectories to calculate the potential temperature (θ) to reveal the diabatic heating that occurs as air approaches the heatwave region. The potential temperature along the trajectories was calculated as in Eq. (1), where p_0 is the reference pressure of 1000 hPa and $\kappa = R/c_p = 0.286$ (R is the gas constant of dry air and c_p is the specific heat capacity).

$$\theta = T(p_0/p)^{\kappa} \quad (1)$$

The trajectories were initiated from the geographical centre of heatwave events such that there is one trajectory per heatwave day starting at 12 p.m. local time, and 950 hPa. This approach was used so that each trajectory is a reasonably independent sample of a heatwave day. We identified the co-ordinates for the centre of a heatwave event on any given day as the medians of the latitude and longitude of grid points that experienced an event. We also restricted the sample of heatwaves to large-scale spatial events (at least 9 grid points that occurred within each region in Fig. 1d). This eliminated single grid point events that can arise by chance and are not associated with an anticyclone to the east. Statistical significance in the median of the potential temperature and height of the El Niño and La Niña trajectories was calculated using a bootstrapping method. 10,000 sub-samples of the trajectories were taken with replacement to calculate a 5–95% confidence interval for the median. Significant differences in the median of the El Niño and La Niña experiments occur when their confidence intervals do not overlap. The robustness of the results was also tested against the entire distribution of trajectories (not just the median) using a Kolmogorov–Smirnov test, but similar significance patterns were found.

3 Results

Before analysing the effect of ENSO on the three mechanisms described in the introduction, we examine the ensemble means of heatwave frequency, duration and amplitude for El Niño and La Niña (Fig. 2). El Niño has approximately eight more heatwave days on average than the control simulation climatology, and La Niña can have about six fewer heatwave days on average (Fig. 2a, d). Statistically significant differences for frequency occur in the northwest, central inland and eastern areas of Australia for El Niño and most northern regions for La Niña. The duration of the longest heatwave (Fig. 2b, e) shows a similar pattern to frequency, with El Niño heatwaves being 2 days longer and La Niña being 2 days shorter than the control simulation. ENSO's influence on heatwave amplitude (Fig. 2c) is less spatially uniform but heatwaves are generally warmer during El Niño in the southeastern region with a small area of relatively weaker heatwaves in the western side of southeast Australia. This pattern is approximately reversed during La Niña (Fig. 2f). However, the impacts of ENSO on heatwave amplitude are not statistically significant.

It is clear that the impacts of ENSO forcing on summer heatwave frequency and duration is prevalent for the north and eastern regions of Australia, typical of the observed impacts of ENSO from other studies (Perkins 2015; Loughran et al. 2017a). The spread of the ensemble members also varies across the north, northeast, east and southeast. Figure 3 demonstrates this by showing the area averaged number of heatwave days for each region in Fig. 1d. In the north and northeast regions, El Niño has a wider spread of heatwave days, while La Niña consistently has fewer. On the other hand, the eastern region has a broader spread during La Niña, and the southeastern region has a similar range of heatwave seasons between El Niño and La Niña. To examine how these impacts might arise, we will focus on each of the three mechanisms from the introduction in more detail.

3.1 Surface energy balance and atmospheric heating

Figure 4a, b show the Q_H and Q_E November–March climatology for the control simulation, which demonstrates where in Australia sensible or latent heat fluxes are largest. Q_H ranges from 105 W m^{-2} in the southwest to 60 W m^{-2} in the northeast (Fig. 4a). The Q_E has greater variation across the continent: it is smallest in the southwest regions (15 W m^{-2}) and increases gradually in a northeasterly direction, reaching a maximum of 100–120 W m^{-2} along the north and east coast of Australia (Fig. 4b). The greater soil moisture availability is driven by the nearby tropical conditions and the warm East Australian Current and this leads to higher precipitation and Q_E (eg. Chambers et al. 2014; Pepler et al. 2016).

The difference between the ensemble means of the El Niño and La Niña experiments (Fig. 4c, d), shows how Q_H and Q_E vary with the ENSO phase. The El Niño ensembles tend to have a higher Q_H across the eastern half of Australia

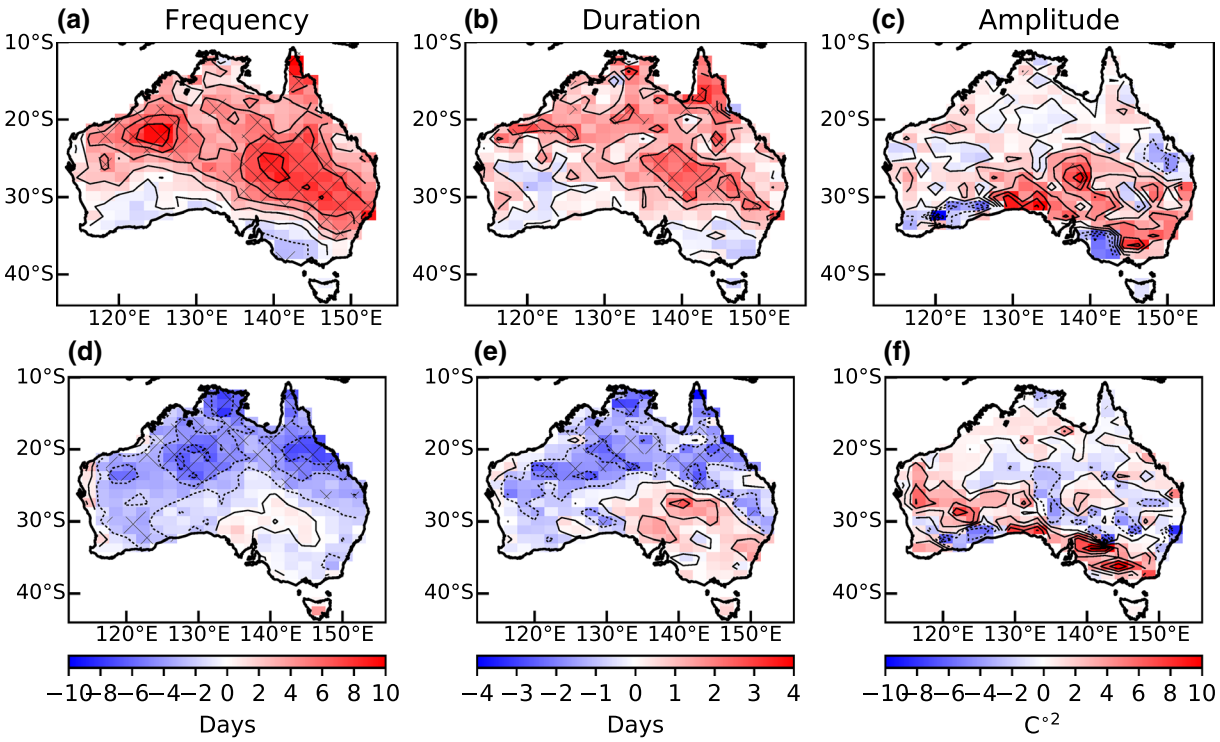

Fig. 2 Ensemble means of heatwave aspects for **a**–**c** the El Niño experiment and **d**–**f** the La Niña experiment. Heatwave frequency is on the left (days), duration is the middle (days), and amplitude is on the right ($C^{\circ 2}$). Dotted contours indicate negative values. T-test statistical significance at the 5% level is indicated with cross hatching

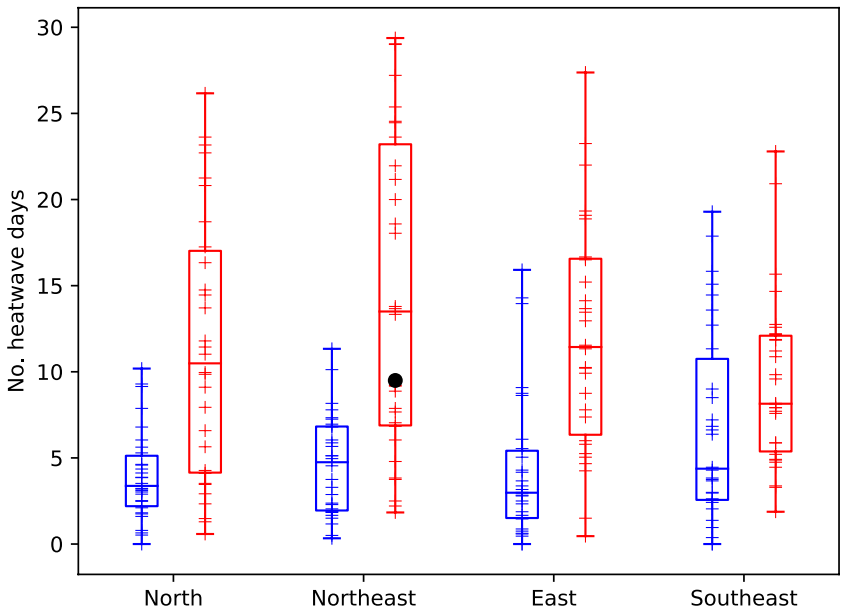

Fig. 3 Box and whisker plots depicting the ensemble spread of the number of heatwave days in each experiment, area averaged over each region in Fig. 1d. Red indicates the El Niño experiment and blue are the La Niña experiment. The black dot marks the control simulation climatology averaged for the northeastern region

(12 W m^{-2} in the southeast and 24 W m^{-2} in the northeast, see Fig. 4c). This corresponds to a decrease in Q_E (−8 W m^{-2} in the southeast and −20 W m^{-2} in the northeast, see Fig. 4d). The changes to Q_E and Q_H in the western half of Australia are opposite, but much smaller in comparison to those in the east. In short, El Niño re-partitions the surface energy balance towards higher Q_H and less Q_E over the eastern parts of Australia, increasing the rate the surface warms the atmosphere which in turn tends to lead to warmer summers and the potential for more heatwaves.

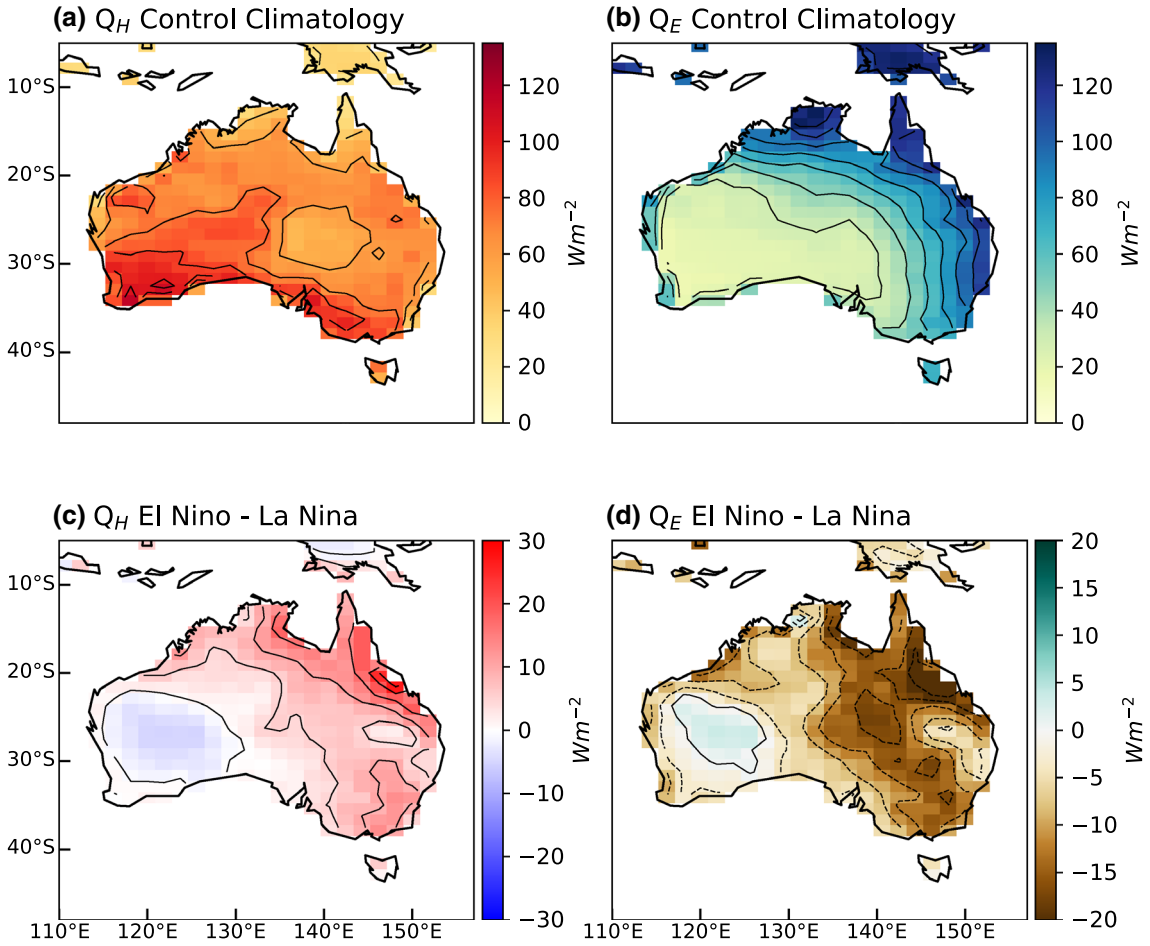

Fig. 4 November–March means from the control simulation for **a** sensible heat flux (contouring 20 W m^{-2} intervals), **b** latent heat flux (contouring every 20 W m^{-2} intervals), and **c, d** the corresponding differences between the ensemble means of the El Niño and La Niña experiments expressed as anomalies from the control simulation climatology. Dashed contours indicate negative values where the El Niño ensemble mean is less than the La Niña ensemble mean

Compared to the reanalysis, the variability of Q_H and Q_E in the model experiments is similar despite the existence of some climatological bias in the model. Figure 5a shows that the 20CR Q_H November–March climatological mean is approximately 100 W m^{-2} in the north and northeast, which is much higher than ACCESS. There is also slightly less Q_E in the reanalysis (Fig. 5b), although the spatial pattern is the same. Nevertheless, the difference between El Niño and La Niña years in the reanalysis (Fig. 5c, d) is similar to the model in spatial pattern and magnitude.

To examine these effects on heatwaves we will also explore the changes in surface heat fluxes that occur specifically on heat wave days. Figures 6 and 9 show the Q_H in ACCESS and 20CR composited for heatwaves that occur in the four regions shown in Fig. 1d, while Figs. 7 and 10 show the same for Q_E. The change in heat fluxes on heatwave days is characterised by significant and highly localised increases in Q_H around the heatwave region and moderate decreases elsewhere. In the north of Australia, this change is much larger in La Niña phase than El Niño (compare 30–50 W m^{-2} in Fig. 6a, b). As we look at regions in the northeast and moving south the magnitude of Q_H increase become more similar between El Niño and La Niña (Fig. 6c, e, g and d, f, h).

The above increases in Q_H correspond to decreases in Q_E. The ACCESS Q_E composites on heatwaves days in Fig. 7 show significant and localised decreases in Q_E which mirror the anomalies in Fig. 6. For example, the anomalies for heatwaves occurring in the north are approximately − 30 W m^{-2} in El Niño and − 50 W m^{-2} in La Niña (Fig. 7a, b), which is proportional to the increases in Q_H. This means that on heatwave days the energy balance favours sensible heating which contributes to higher air temperatures. The larger heat flux anomalies in the La Niña experiments suggests that during La Niña strong surface heating is an important component in order to generate the extreme temperatures in otherwise adverse conditions as demonstrated in Fig. 2.

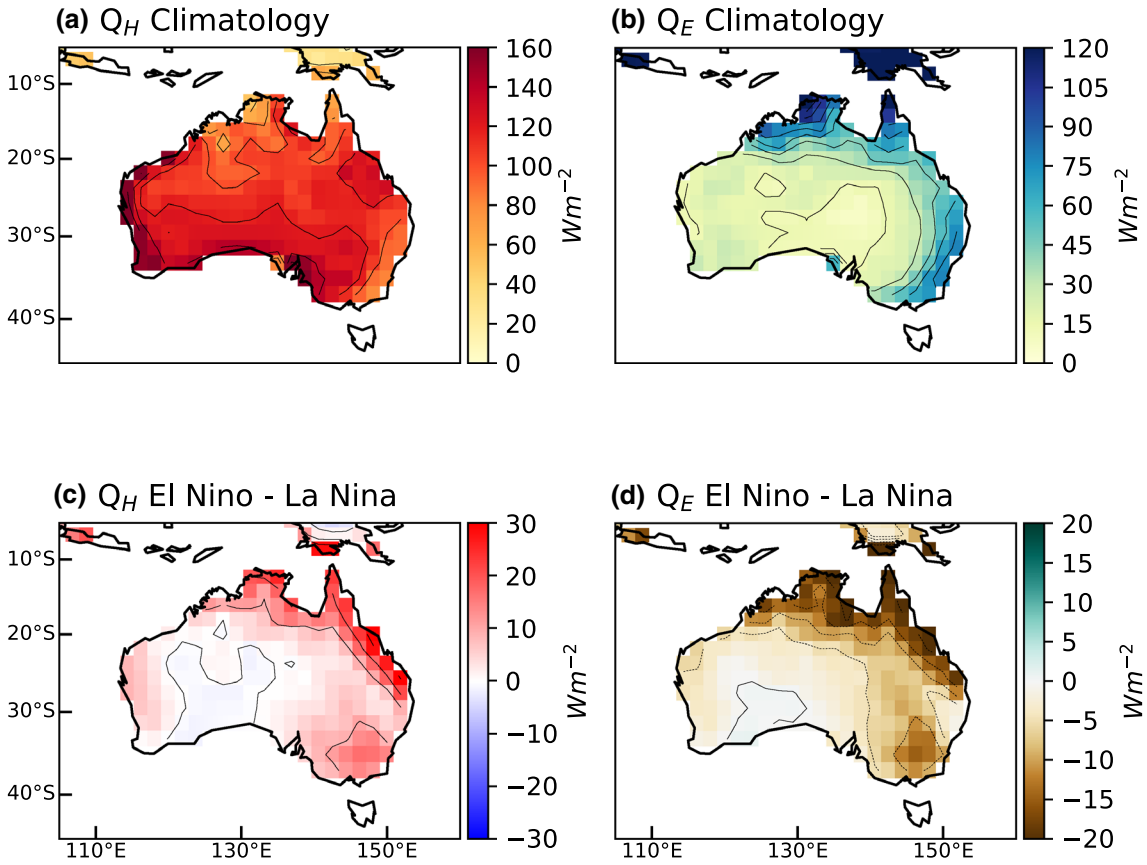

Fig. 5 Reanalysis November–March 1960–2012 means for **a** sensible heat flux (contouring 20 W m^{-2} intervals), **b** latent heat flux (contouring every 20 W m^{-2} intervals), and **c, d** the corresponding differences between the means of the El Niño and La Niña years expressed as anomalies from the climatology. Dashed contours indicate negative values where the El Niño mean is less than the La Niña mean

Compared to the north and northeastern regions, the east and southeast regions show some displacement in heat flux anomalies from the region where the heatwaves occur. The eastern region heat flux anomalies are situated slightly north from the respective compositing box (e.g. Figs. 6e, f, 7e, f). The southeast regions anomalies are the weakest of all the regions and are situated to the northeast of its respective compositing box (Figs. 6g, h, 7g, h). This may indicate a change in the dominant processes responsible for the development of the heatwaves. That is, the heatwaves in the east and southeast accumulate their heat from sensible heating in the north or northeast which is then advected towards the heatwave region driven by the Tasman Sea anticyclone. This is consistent with the findings of Quinting and Reeder (2017) who used similar trajectory analysis to identify that air masses advecting into heatwaves in southeastern Australia accumulate their heat from remote regions.

For all but the southeast region, there are more than double the number of heatwave days in the El Niño experiment compared to the La Niña experiment. For example, the eastern region has 255 heatwave days for the El Niño experiment, while the La Niña experiment had only 95. On the other hand, the southern region has 204 heatwave days for El Niño, and the La Niña experiment has not much fewer with 196 days. This agrees with observational studies that ENSO has relatively little influence on the number of heatwave days in the southeastern region (Boschat et al. 2014; Parker et al. 2014b).

While results from the La Niña experiments fairly consistently yield very few heatwave days, an El Niño event does not necessarily guarantee a summer season with more than average heatwave days (Fig. 3). The reason a given El Niño event has fewer than expected heatwaves may be because the soil is moist and the surface energy balance is dominated by Q_E rather than Q_H. Figure 8 shows the Q_H, Q_E and soil moisture of the differences between the summer ensemble means of 11 El Niño ensembles that had fewer heatwave days than the climatology in the northeast and the remaining 19 that had more (see black dot in Fig. 3). This demonstrates that for El Niño summers that have fewer than average heatwaves, there is a decrease in the Q_H (Fig. 8a) and an equivalent increase in Q_E (Fig. 8b), which is associated with an increase in the available surface soil moisture (Fig. 8c) and precipitation (Fig. 8d) (Seneviratne et al. 2010).

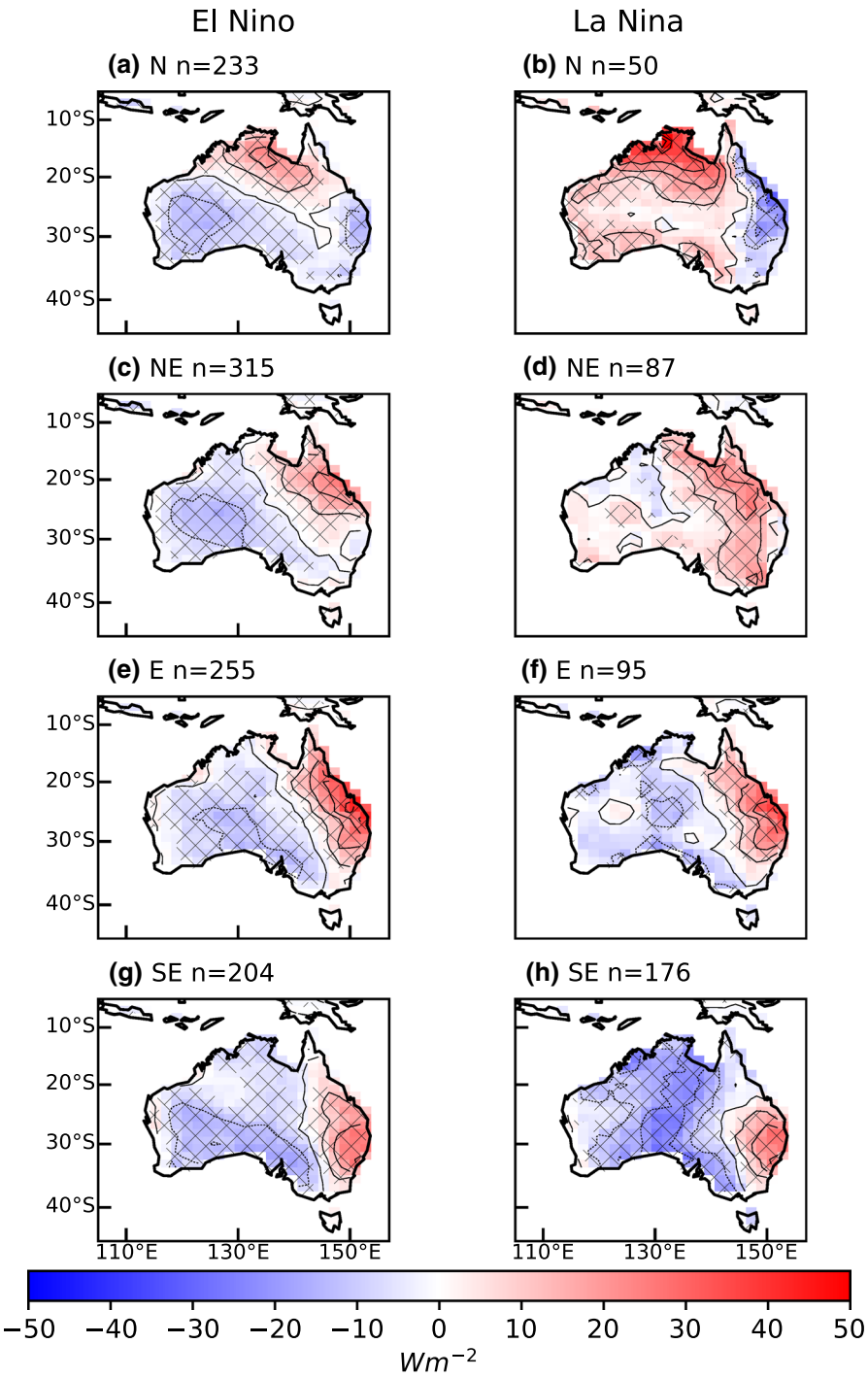

Fig. 6 Modelled composites of sensible heat flux (both shading and contours at 10 W m^{-2} intervals) for heatwave days in **a, b** the north, **c, d** northeast, **e, f** east, and **g, h** southeast (see the rectangles in Fig. 1d). Values are expressed as anomalies from the control simulation climatology. The El Niño experiment is on the left and the La Niña experiment is on the right. The 'n' numbers in the top of each plot are the number of heatwave days used in each composite

Clearly, the concurrent and antecedent soil moisture conditions are important for predicting the association between ENSO and extreme heat in a given season (Kala et al. 2015).

In order to compare the effect of ENSO on Q_H and Q_E in ACCESS and observations, the observed heat fluxes from 20CR on heatwave days are shown in Figs. 9 and 10. They show general agreement in sign with the model simulations, but sometimes disagree with the simulations in the precise spatial distribution. For example, Fig. 9 shows that the northern region has weak local changes to Q_H in El Niño and strong increases in the northeast in La Niña (Fig. 9a, b), however the robustness of this is poor as it consists of only six heatwave days from two heatwave events. The northeastern region has a similar pattern, but weaker anomalies due to a slightly larger sample of heatwave days (Fig. 9c, d). The east and southeast regions contrast with the simulations especially during La Niña. Generally, Q_H during El Niño on heatwave days is higher

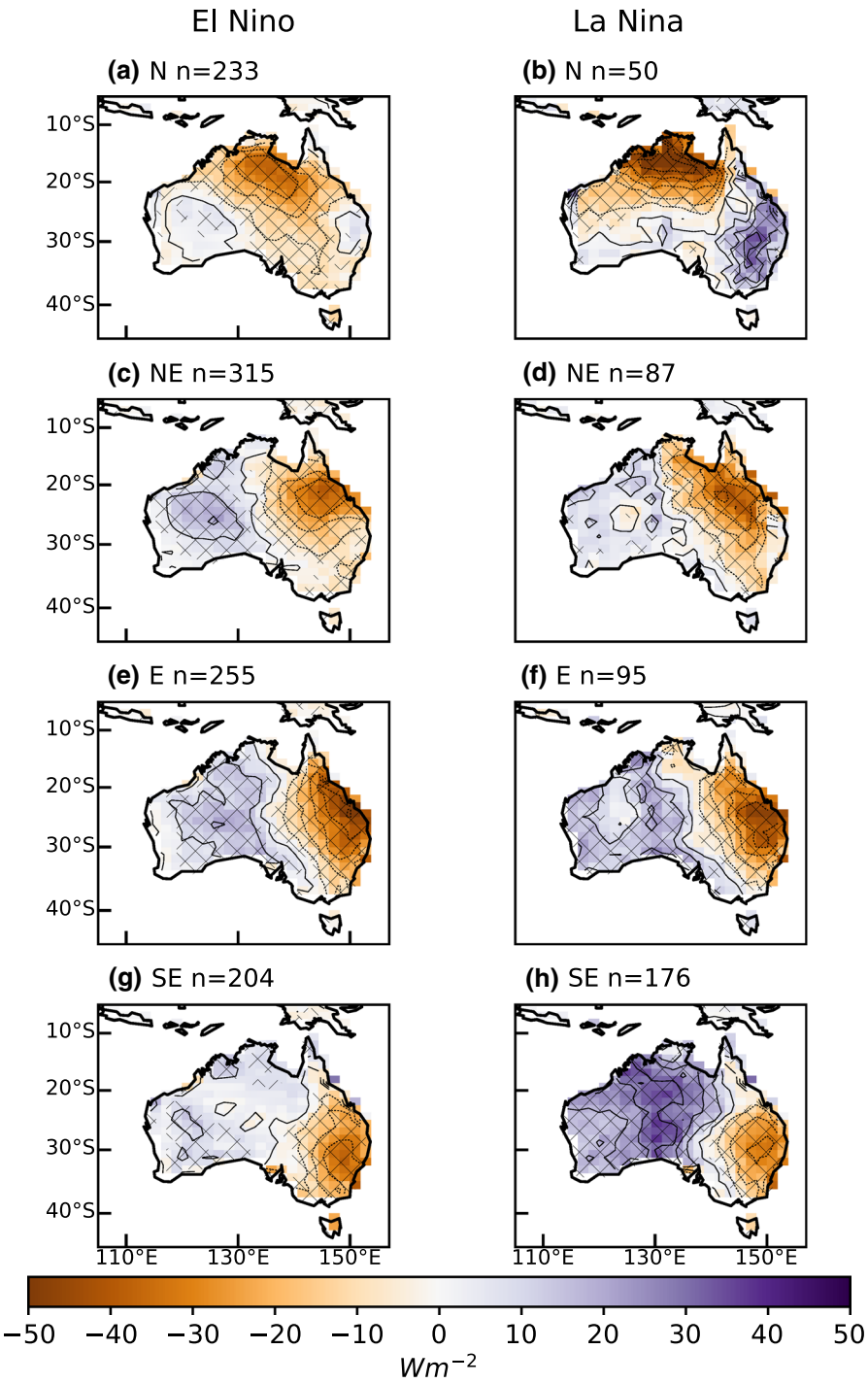

Fig. 7 Modelled composites of latent heat flux (both shading and contours at 10 W m^{-2} intervals) for heatwave days in **a, b** the north, **c, d** northeast, **e, f** east, and **g, h** southeast (see the rectangles in Fig. 1d). Values are expressed as anomalies from the control simulation climatology. The El Niño experiment is on the left and the La Niña experiment is on the right. The 'n' numbers in the top of each plot are the number of heatwave days used in each composite

than normal and less than normal during La Niña (Fig. 9e, h).

The observed Q_E on heatwave days is more consistent with ACCESS but still contrast somewhat with the simulations. Figure 10a–d shows significant decreases in Q_E for both El Niño and La Niña for heatwaves occurring the north and northeast. However, for heatwaves occurring in the southeast and eastern regions, the Q_E is less during El Niño and generally not significant during La Niña (Fig. 10e–h). The number of heatwave samples in the observations is much less than the simulations per ENSO phase. Additionally, there is greater spread (not shown) of Q_H and Q_E in the observations which would interfere with identifying a difference between El Niño and La Niña. Another factor is a variety of strong and relatively weak ENSO events in observations, while in the ACCESS experiments the ENSO events are all the same.

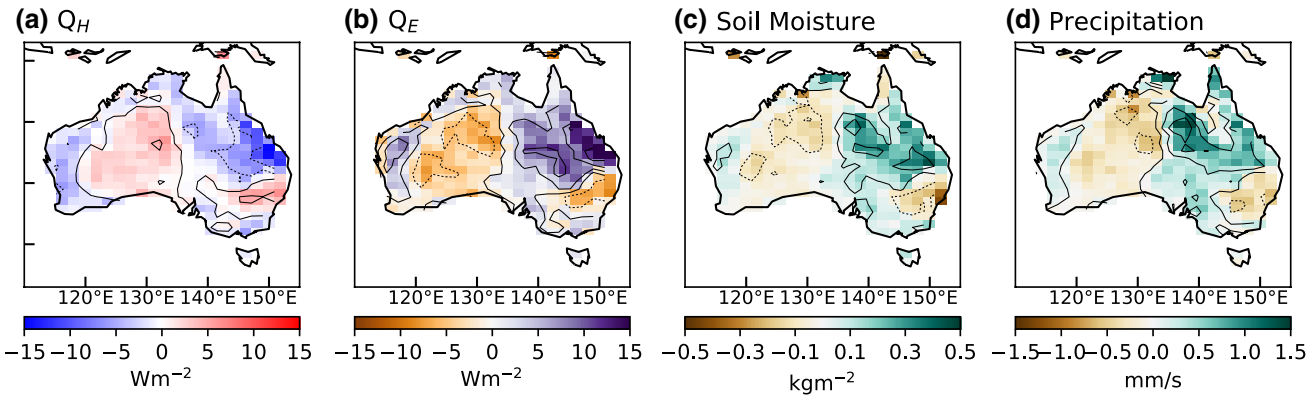

Fig. 8 November–March mean difference of the below average north-eastern heatwave frequency El Niño ensemble members from the above average El Niño members, for **a** sensible heat flux (contouring interval 5 W m^{-2}), **b** latent heat flux (contouring interval 5 W m^{-2}), **c** surface level soil moisture (contouring interval 0.2 kg m^{-2}) and **d** precipitation (contouring interval 0.5 mm s^{-1})

To summarise, the El Niño experiment exhibited higher climatological atmospheric warming than La Niña linked with the re-partitioning of the surface energy balance to increased Q_H and decreased Q_E, which led to more heating of the lower atmosphere and therefore a tendency to more extreme temperatures. On heatwave days specifically, the northern region had much larger Q_H and lower Q_E during La Niña. This was likely due to the importance of soil moisture in the region, which tends to suppress heatwave development even during El Niño when other conditions might be conducive to heatwave development. This effect could be seen in the observations to some extent, however there were several points of disagreement in the southern regions of Australia, and the lack of samples in observations would make conclusions tenuous.

3.2 Synoptic anticyclones and horizontal advection

We now examine the synoptic pressure systems that occur during heatwaves in each ENSO phase and how they might affect the synoptic patterns advecting heat towards each heatwave region. Figure 11 shows the synoptic MSLP anomaly patterns composited for heatwave days in each ENSO phase and region. The synoptic pattern associated with heatwaves depends on the region. During El Niño, heatwaves in the north, northeast and east (Fig. 11a, c, e) are characterised by anomalously high pressure to the northeast, and low pressure to the south. The La Niña phase does not feature high pressure to the north, but tends to maintain the low over the Southern Ocean (Fig. 11b, d, f). The lack of a consistent synoptic high anomaly in these regions for the La Niña experiment is due to the dominance of the Southern Oscillation on the pressure field. The composite for northern Australian heatwaves (Fig. 11b) also has a large high pressure system southeast of New Zealand, though it should be noted that this composite contains only 50 heatwave days. There are broad regions of high pressure in the Indo-Pacific region during El Niño and relatively lower pressure in the central equatorial Pacific, driven by the SST forcing. This pattern is reversed in the La Niña experiments. This might suggest that winds would flow from the west–northwest and the interior of the continent, but low latitude winds seldom follow the geostrophic balance. The corresponding wind barbs that are overlaid in Fig. 11 indicate that air flow is generally from the east, usually associated with a mid-latitude anticyclone.

On the other hand, the southern region is dominated by an anticyclone situated over the Tasman Sea, geostrophically advecting air from the north and northeast (Fig. 11g, h). The high anomaly tends to be weaker in the La Niña experiment, helping to account for the fewer heatwave days compared to El Niño. For this region, the anomalies are generally only statistically significant in the subtropics and extratropics, which suggests that Southern Oscillation related subsidence and convection is unrelated to heatwaves in the southeast.

The MSLP patterns derived from 20CR are inconsistent with the simulations, likely because of the poor sample sizes. The MSLP associated with heatwaves in the northern region are weak and mostly not significant (Fig. 12a, b). The northeast and eastern region composite shows the increased pressure surrounding the northern parts of Australia associated with the El Niño phase of the Southern Oscillation, but the La Niña phase does not (Fig. 12c–f). The eastern and southeastern region La Niña phase does display the Tasman anticyclone (Fig. 12f, h), but not in the El Niño phase.

To summarise, the effect of ENSO on winds and pressure systems related to heatwaves, the phase of ENSO can weakly affect the pressure field near Australia through the action of the Southern Oscillation. But this would only affect the northern region, and does not much affect the positioning of the synoptic patterns that would advect warm air towards the heatwave. The Southern Oscillation and extratropical Rossby wave structures could not be consistently identified based on

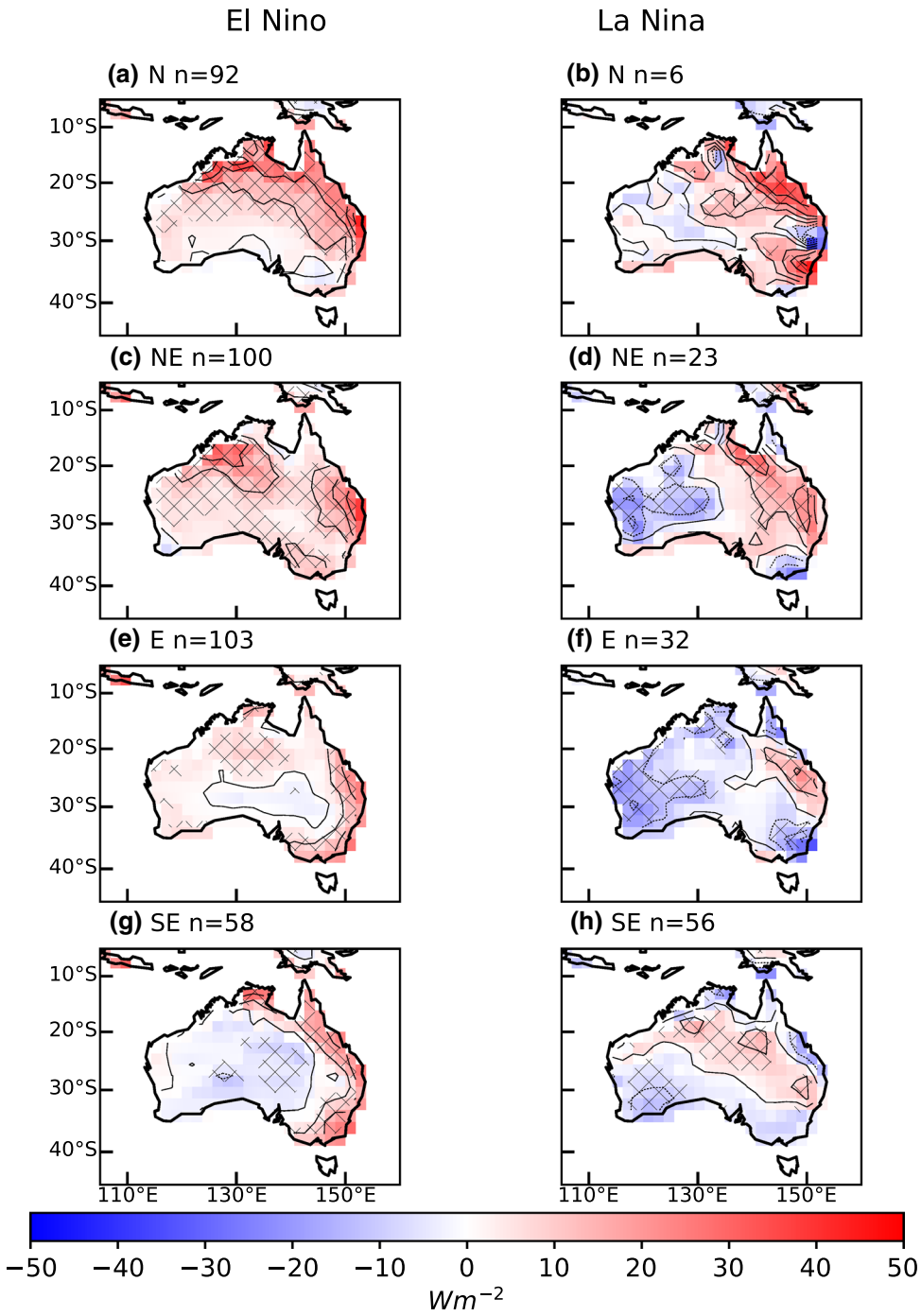

Fig. 9 Observed, composites of sensible heat flux (both shading and contours at 10 W m^{-2} intervals) for heatwave days in **a, b** the north, **c, d** northeast, **e, f** east, and **g, h** southeast (see the rectangles in Fig. 1d). Values are expressed as anomalies from the November–March, 1901–2012 climatology. The El Niño years are on the left and the La Niña years are on the right. The 'n' numbers in the top right of each plot are the number of heatwave days used in each composite

20 CR MSLP due to small heatwave sample sizes and inconsistent ENSO variations, hindering the observation of changes to these structures for each phase. Therefore, it does not appear that ENSO could influence heatwave development by geostrophically advecting air from different regions.

3.3 Analysis of subsiding heat using back trajectories

While ENSO may have little effect on the synoptic structures, it may still impact the vertical movement of air

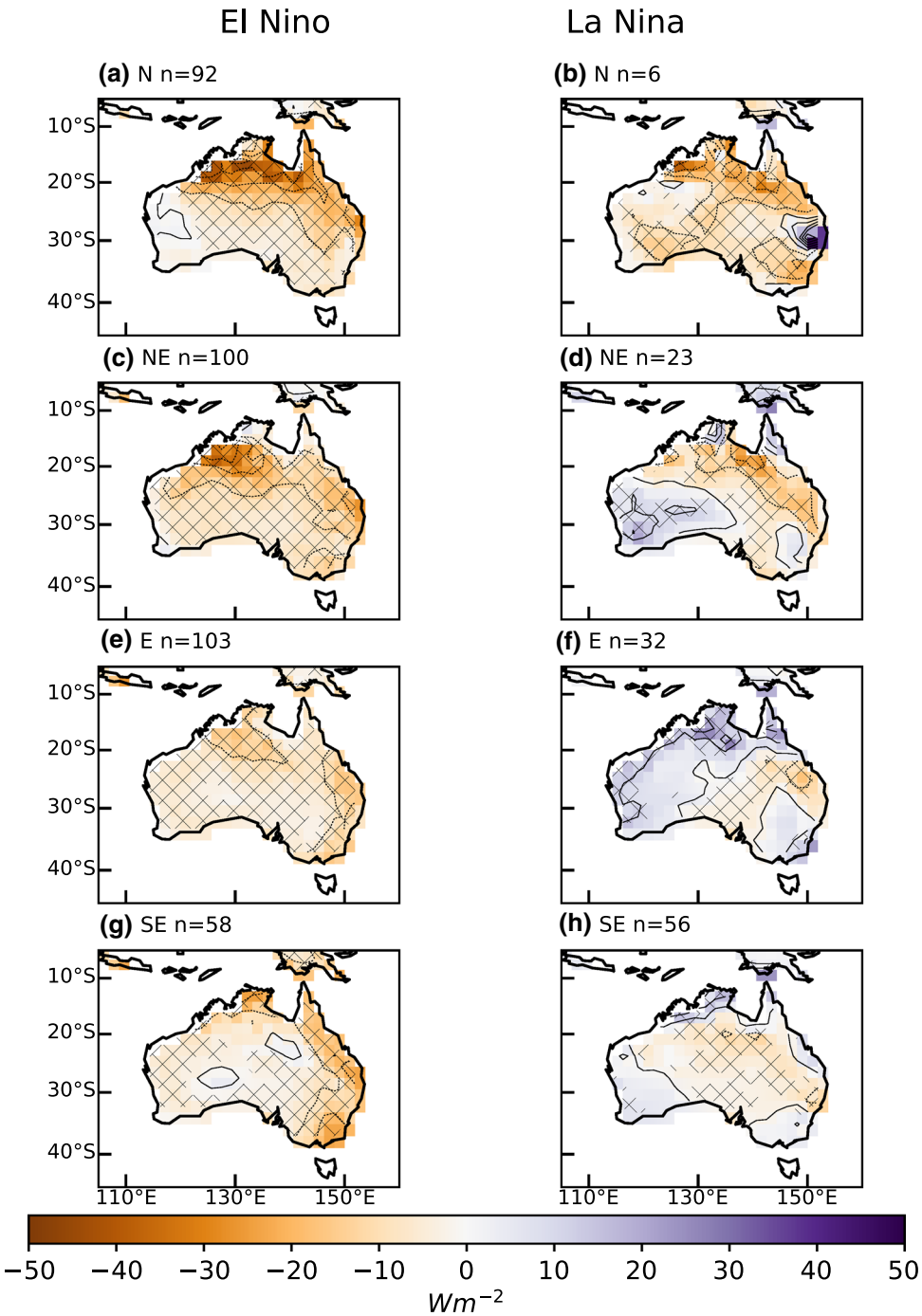

Fig. 10 Observed composites of latent heat flux (both shading and contours at 10 W m^{-2} intervals) for heatwave days in **a, b** the north, **c, d** northeast, **e, f** east, and **g, h** southeast (see the rectangles in Fig. 1d). Values are expressed as anomalies from the November–March, 1901–2012 climatology. The El Niño years are on the left and the La Niña years are on the right. The 'n' numbers in the top right of each plot are the number of heatwave days used in each composite

which can contribute to a large amount of warming to the heatwave adiabatically. Figure 13 shows the tracks of the air parcels up to 10 days before the heatwave events for each ENSO phase and region, demonstrating where air parcels come from and where they descend. There are fewer trajectories than the heatwave days sampled in the composites because some heatwave events did not meet the requirement of at least nine grid points in size, or because the trajectory scheme advected the parcel below the surface of the earth and terminated it. This mostly affected trajectories for heatwaves in the northern region. Heatwaves in northern Australia (Fig. 13a, b) have air masses approach the heatwave region from the south to southeast, descending as they move north. Prior to that, the origins of air for northern heatwaves can be from the Pacific Ocean to the east or from far to the south. There does not seem to be a consistent path taken by air approaching northern heatwaves, but future studies may benefit from a trajectory clustering analysis if more samples are available (e.g. Harpaz et al. 2014).

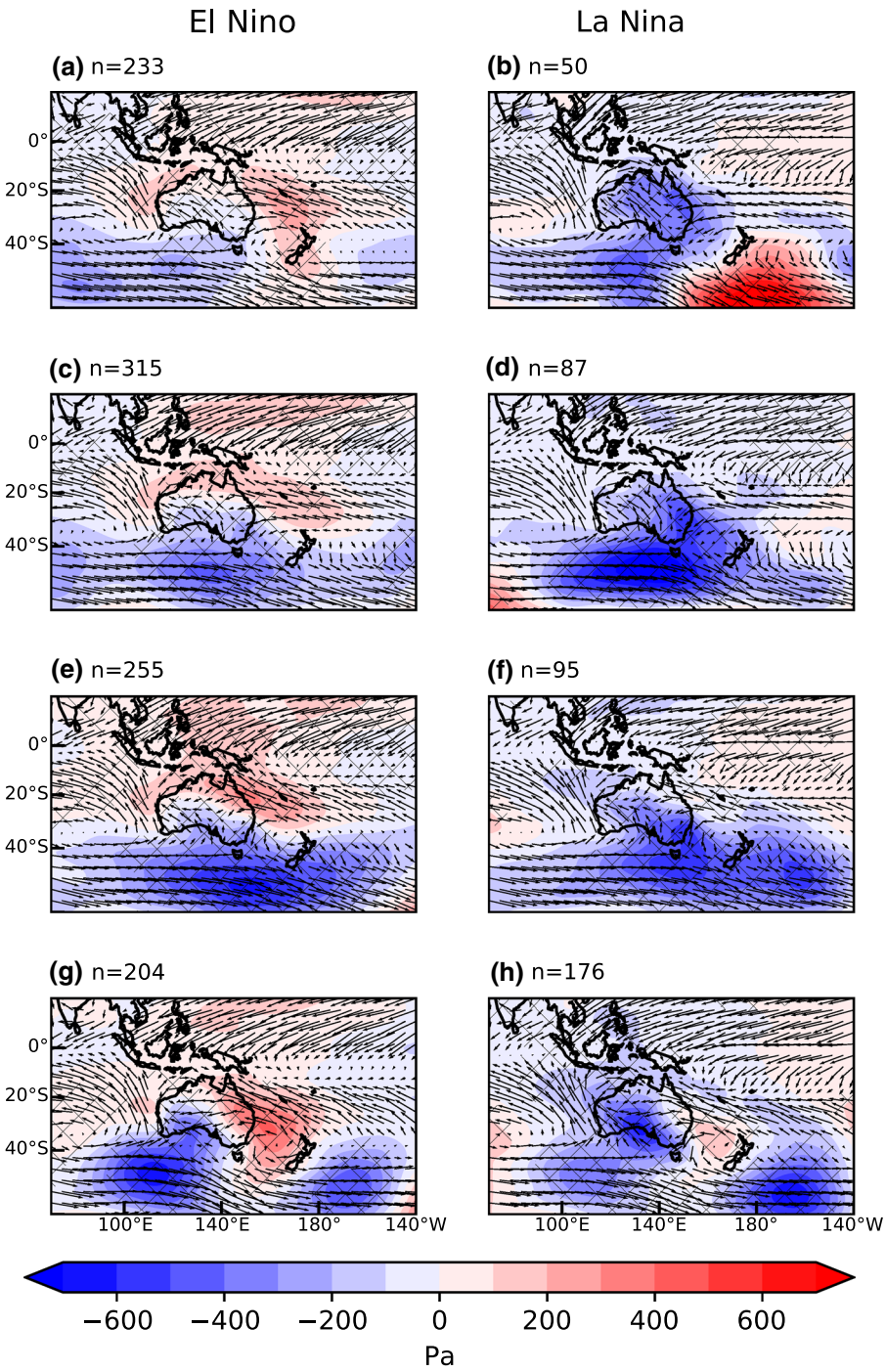

Fig. 11 Modelled mean sea level pressure anomaly (Pa, contours at 100 Pa intervals) composites for heatwave days in **a, b** the north, **c, d** northeast, **e, f** east, and **g, h** southeast. Values are expressed as anomalies from the control simulation November–March climatology. Contouring interval is 200 hPa. The El Niño experiment is on the left and the La Niña experiment is on the right. The numbers in the top right of each plot are the number of heatwave days used in each composite

For heatwaves in the northeast, eastern and southeastern regions (Fig. 13c–h) air approaches the heatwave from the north or northeast. These air masses originate from the Tasman Sea and rotate and descend around an anticyclone before arriving at the heatwave location. Most of the trajectories originate from the westerly winds anywhere between 800 and 400 hPa over the Southern Ocean. Many of them can circulate beyond New Zealand and over the south Pacific before approaching the heatwave in Australia. There appears to be no ENSO related difference in the horizontal origins of heatwave air for North and Northeastern heatwaves. However, there does appear to be a difference for the East Australian region (Fig. 13e, f). Many more trajectories originate from the Southern Ocean in El Niño, while more air originates from the South Pacific region during La Niña.

There are some differences in the vertical origins of air between ENSO phases. Figure 14 shows the medians of pressure along the trajectories for each region. The northern

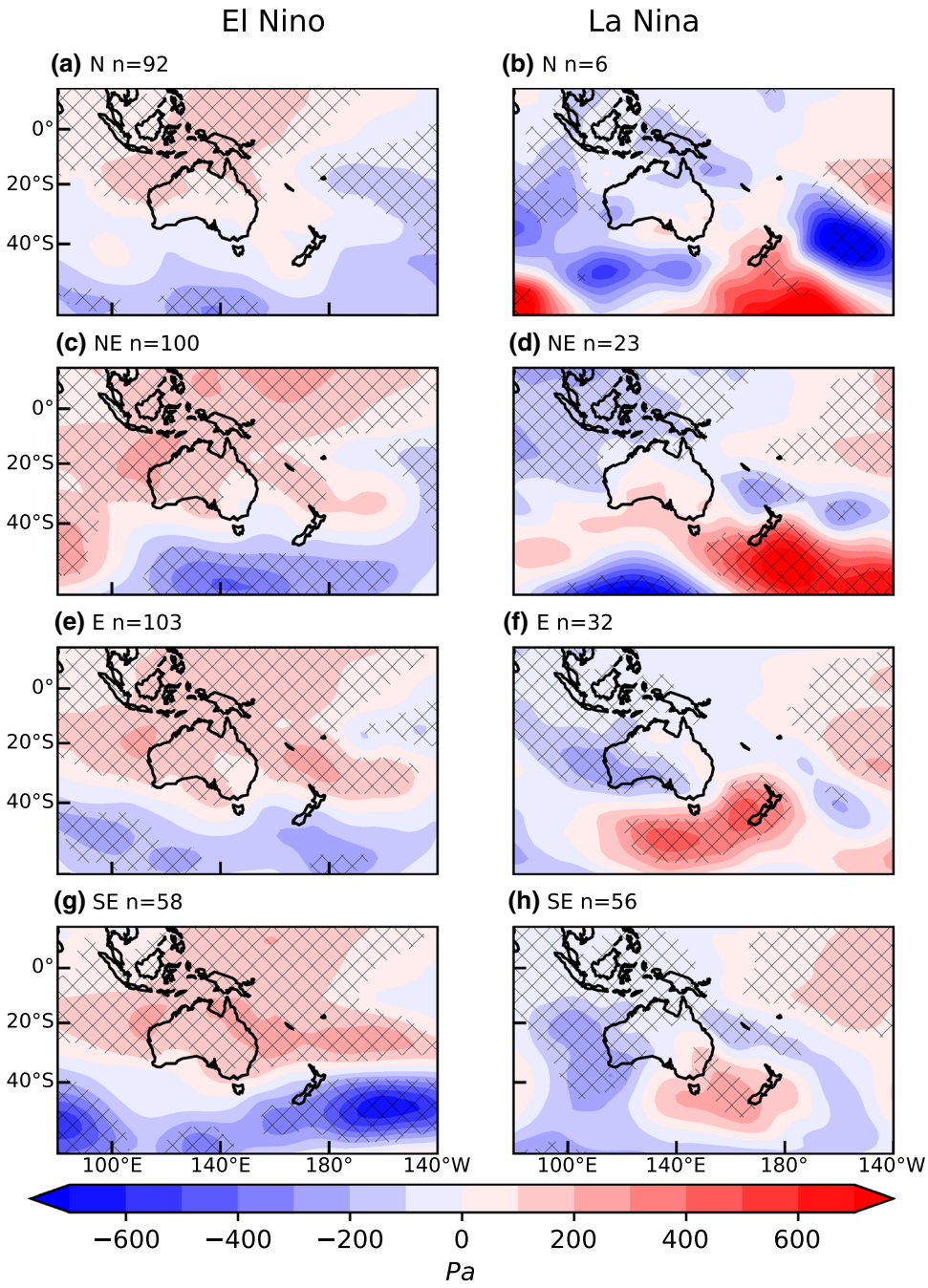

Fig. 12 Observed composites of MSLP (Pa, contours at 100 Pa intervals) for heatwave days in **a, b** the north, **c, d** northeast, **e, f** east, and **g, h** southeast (see the rectangles in Fig. 1d). Values are expressed as anomalies from the November–March, 1901–2012 climatology. The El Niño years are on the left and the La Niña years are on the right. The numbers in the top right of each plot are the number of heatwave days used in each composite

region does not show any significant differences in height (Fig. 14a). In the last 5–6 days before the heatwave, the air pressure level shows few significant differences between the ENSO phase. During days 10–6, heatwaves in the northeast tend to have air originate from lower in the atmosphere during El Niño (Fig. 14b). On the other hand, in the east and southeastern heatwaves region, air tends to originate from lower in the atmosphere during La Niña (Fig. 14c, d). This could be due to differences in the origins of air being advected into the Tasman Sea anticyclone, which may account for the differences in height. That is, during El Niño air originates from high over the Southern Ocean and descends in the Tasman anticyclone. On the other hand, during La Niña westerly flowing air enters the anticyclone from the subtropical ridge over the South Pacific at slightly lower latitudes and altitudes, where the climatological South Pacific anticyclone is stronger during La Niña, or weaker during El Niño (Trenberth 1976; Rasmusson and Carpenter 1982).

The adiabatic warming and diabatic heating that occurs to the air along the trajectories can be seen in the potential temperature in Fig. 15. Potential temperature at days

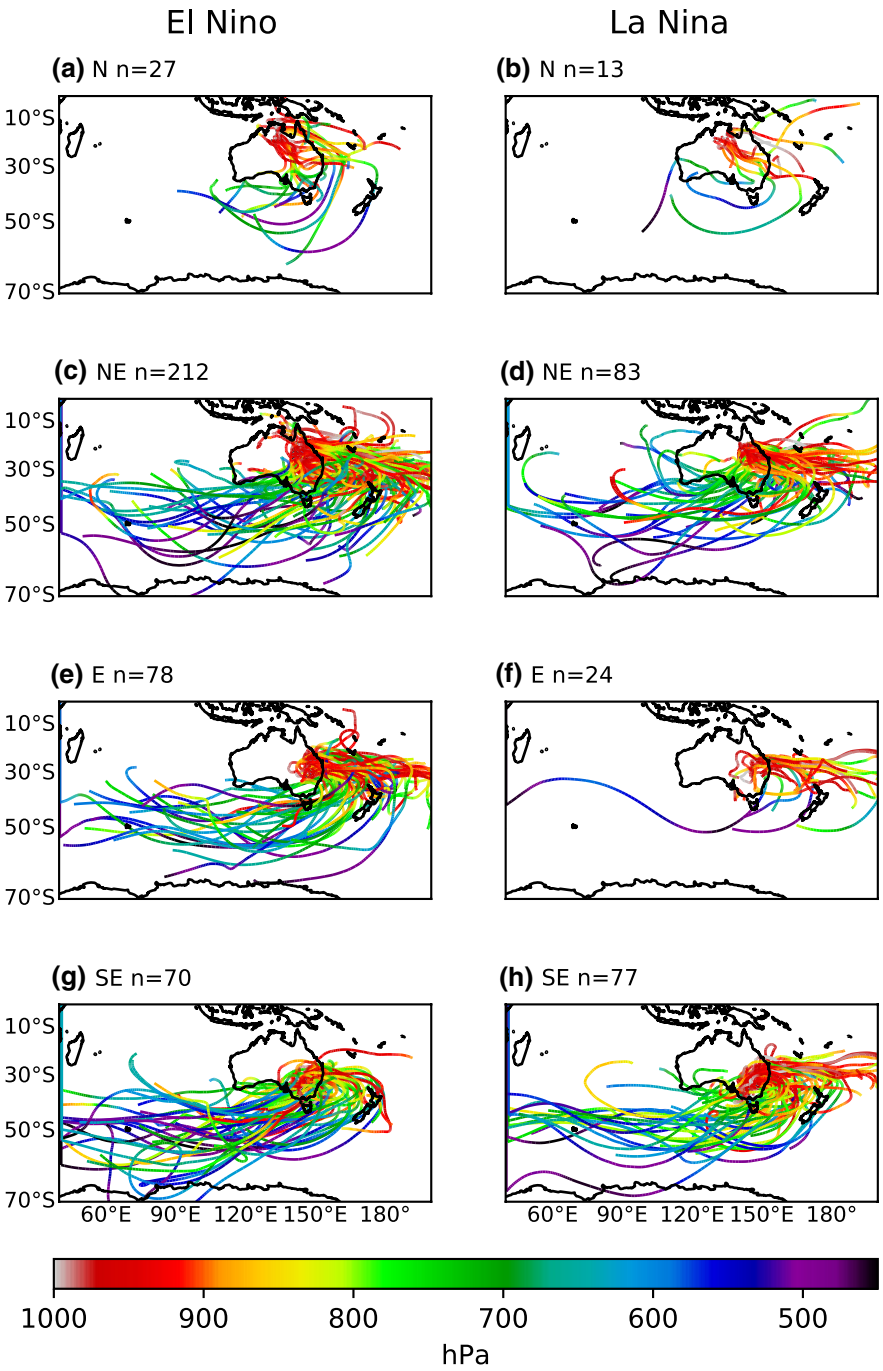

Fig. 13 10 day backward air parcel tracks for heatwave events in the EL Niño (left) and La Niña (right) experiments. Tracks are plotted for each region in Fig. 1d, **a, b** north, **c, d** northeast, **e, f** east, and **g, h** southeast. Line shading indicates the hydrostatic height of the trajectory in hPa

10–4 before the heatwaves undergoes minimal change for all regions. This is the temperature the air would have if it were reduced to 1000 hPa and therefore is the adiabatic component of the heat content of the heatwave. In the last 4 days, the potential temperature increases as it is heated diabatically within the boundary layer, as can be seen by the diurnal oscillations over this period.

There is no significant difference in the median potential temperature between ENSO phases for any region. It is possible that the distribution of potential temperature for one of the experiments could be bimodal. To account for this, a Kolmogorov–Smirnov test was also used to test the entire distribution of heights and potential temperatures, but the non-significance of the results remains, indicating that the distributions between each experiment are not significantly different. If ENSO affected heatwave development by warming the atmosphere globally and hence increasing the amount of potential temperature subsided from aloft, we might expect to see greater baseline potential heat in the El Niño experiments, but we do not see this in our results.

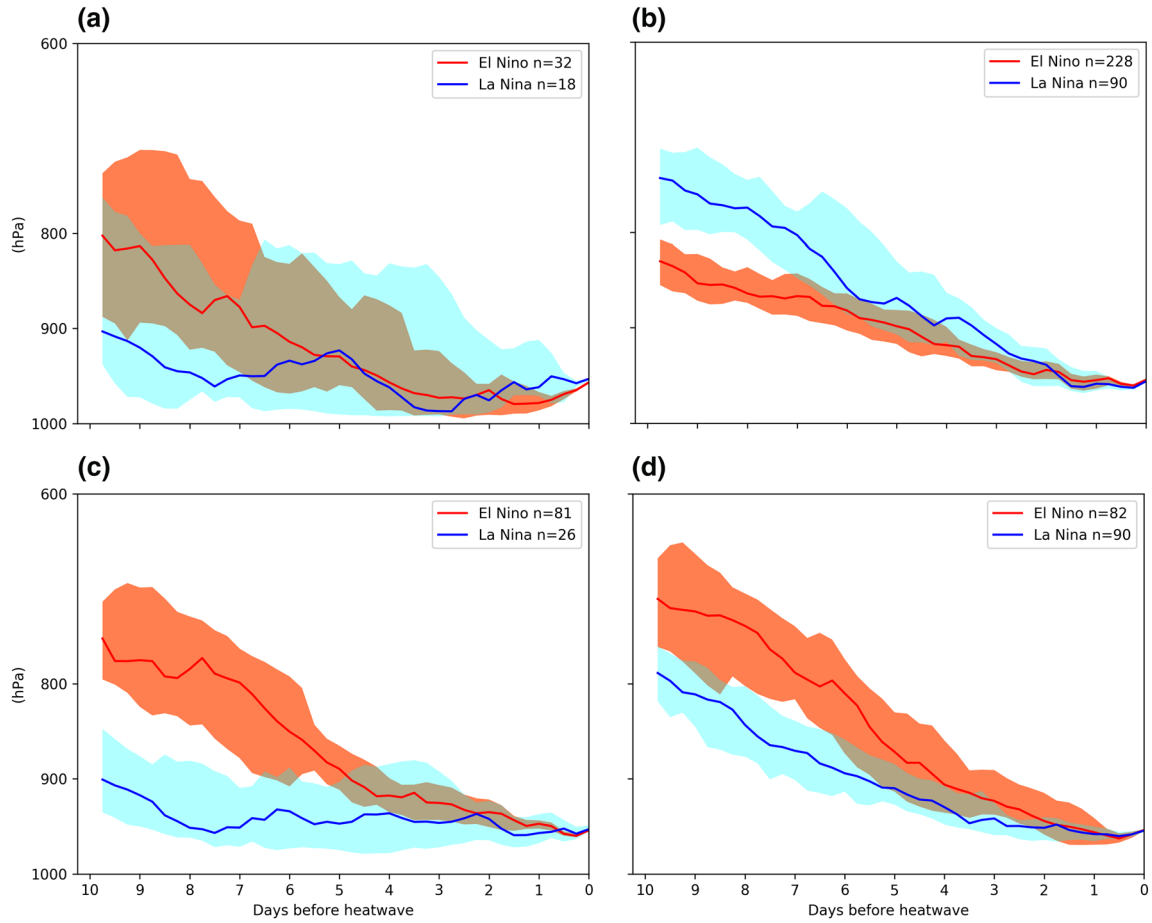

Fig. 14 Median parcel height (hPa) for each ENSO phase along 10 day back trajectories starting at heatwaves in **a** the north, **b** northeast, **c** east, and **d** southeast. Shading indicates the 5–95% confidence interval in the median calculated using the bootstrapping technique. Significant differences in the median between ENSO phase occurs when the confidence intervals do not overlap. The 'n' number in the legend indicates the number of trajectories for each experiment group

4 Discussion and conclusion

We have conducted a 30 member ensemble of ACCESS 1.3 experiments, forced with SSTs containing El Niño and La Niña events, and analysed their effects on three heatwave development mechanisms. The simulations displayed increases in heatwave frequency and duration for northern and eastern Australia during El Niño and decreases for La Niña, similar to the observed impacts of ENSO in Perkins et al. (2015). The El Niño experiments are characterised by summertime decreases in Q_E, compared to the La Niña experiment, which drives more frequent extreme temperatures through sensible surface heating. Meanwhile, maximum heatwave temperatures in the northeast are not significantly different between ENSO phases. On heatwave days, the northern regions of Australia require much larger changes in surface fluxes for a heatwave to occur during the La Niña experiment than El Niño, likely due to the dominating effect of soil moisture in the region and the tendency for wet conditions during La Niña. In fact, existing soil moisture conditions can potentially suppress heatwaves in the northeast, regardless of the occurrence of an El Niño. Hence, surface moisture and energy fluxes are an important mechanism through which ENSO modulates the frequency and duration of north and northeast Australian heatwaves. The MSLP patterns and horizontal advection along trajectories showed little difference between each ENSO phase and the direction from which hot air approaches a heatwave depended primarily on which region that was being affected. This was also true for the trajectory analysis on the subsidence of potential temperature, which did not show any significant differences between ENSO phase for the north and northeastern regions. On the other hand, the trajectories from heatwaves in the eastern and southeastern regions showed stronger subsidence during El Niño, but equivalent potential temperature along the trajectories. Because the El Niño trajectories tend to begin from higher altitude there must therefore be more potential heat aloft that is being subsided through the

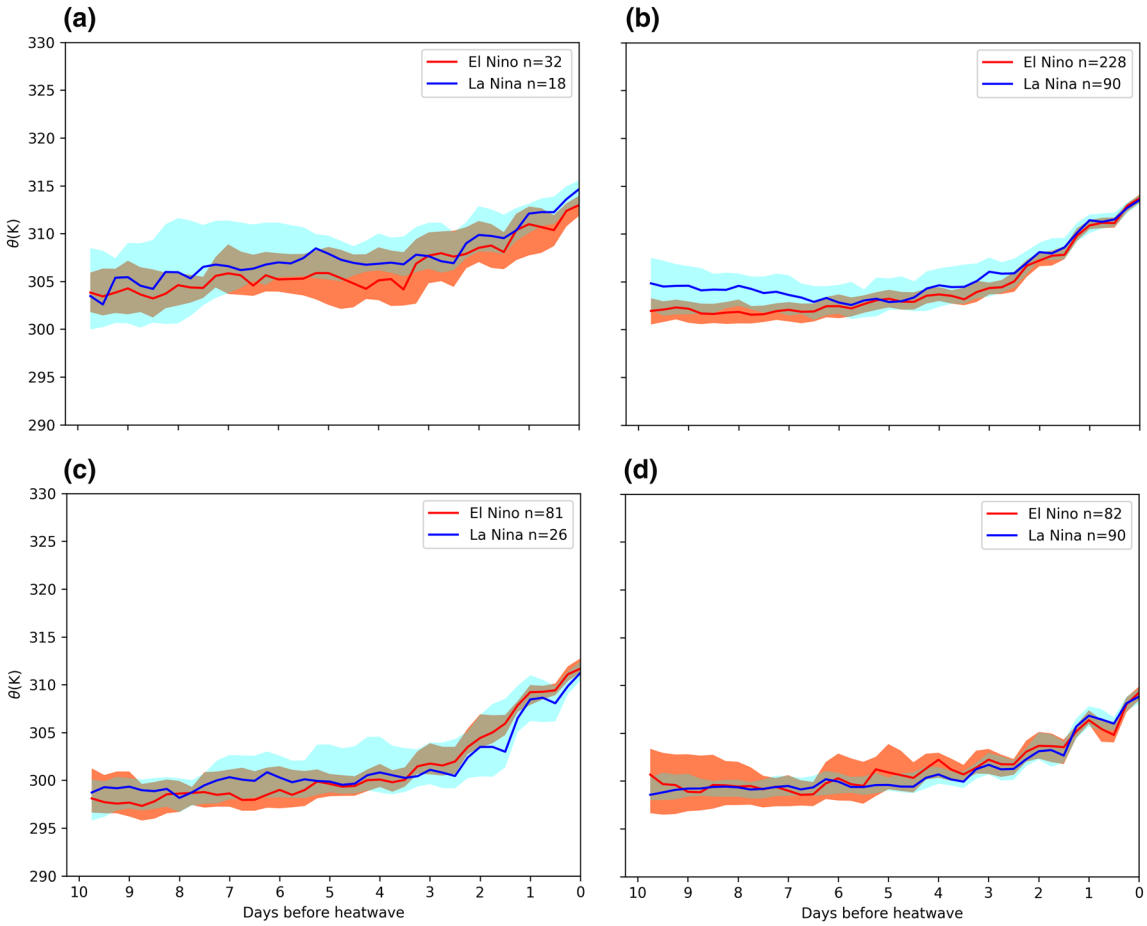

Fig. 15 Median potential temperature (K) for each ENSO phase along 10 day back trajectories starting at heatwaves in the **a** north, **b** northeast, **c** east, and **d** southeast. Shading indicates the 5–95% confidence interval in the median calculated using the bootstrapping technique. Significant differences in the median between ENSO phase occurs when the confidence intervals do not overlap. The n number in the legend indicates the number of trajectories for each experiment group

anticyclone. The difference in the subsidence during each ENSO phase is also evident in the horizontal origins in heatwave air parcel trajectories, whereby air parcels originating from midlatitudes experience stronger adiabatic warming due to the poleward tilt of the isentropes, compared to those originating from the subtropics (Fig. 13e, f).

We recognise that caution needs to be applied in interpreting our finding that the La Niña phase must have stronger diabatic surface heating in order for heatwaves to occur. Boschat et al. (2016) argues against the sole use of composite analysis for the formulation of hypotheses, and shows that the spatial pattern of a field produced by composites can often occur without the occurrence of heatwaves. In the context of our study, composite analysis alone cannot infer that the decrease in Q_E anomalies causes the heatwave days, and that the occurrence of the Q_E anomalies does not necessarily mean that a heatwave will occur. It is plausible that a heatwave may not occur despite the existence of dry land surface conditions and strong surface heating of the atmosphere, especially if the conditions do not persist for more than 3 days. As a result, we do not conclude that the decreased Q_E necessarily causes heatwaves, or that the lower Q_E in La Niña causes more heatwaves (clearly the opposite is true, as demonstrated by Fig. 4). Instead, the composites suggest that the decrease in Q_E and enhanced diabatic heating on heatwave days tends to be stronger during La Niña, but there are multiple factors that contribute to the occurrence of heatwaves. The timing and intensity of rainfall is therefore crucial for the suppression or development of heatwaves during each ENSO phase. Nevertheless, there may be many other adverse conditions for heatwaves that account for the decreased occurrence during La Niña, such as a generally cooler atmosphere, or weaker subsidence in the northern region.

There remain some issues with the inconsistency of the observed and modelled heat fluxes, whereby the model produces larger composite anomalies that are more concentrated in a specific region, when compared to the

observations. Firstly, the combined effect of having fewer observed samples, larger variance and inconsistent ENSO events as highlighted in the result section, makes comparing the observed heat fluxes to the models somewhat difficult. Alternatively, the model itself may be overestimating the magnitude and underestimating the spatial extent of the heat flux anomalies. Similar problems would also apply to the composites for MSLP. Therefore, future studies for observed impacts of ENSO on heatwaves should choose an approach (e.g., case studies) that is not affected by averaging of a small number of samples, as is the case for compositing.

An extraneous variable that might influence the occurrence of heatwaves in Australia is the Southern Annular Mode (SAM), which relates to the strengthening and southerly movement of the circumpolar westerlies during the positive phase. This brings cooler, wetter conditions to eastern Australia (Hendon et al. 2007; Risbey et al. 2009; Marshall et al. 2012). Multiple studies have noted a relationship between the ENSO and SAM, whereby the westerlies move south (positive SAM) during La Niña, or north during El Niño (Karoly 1989; Seager et al. 2003; L'Heureux and Thompson 2006). Therefore, the SAM conditions within ACCESS may co-vary with ENSO and also influence the occurrence of heatwaves. Table 1 lists the December–February mean of the SAM using the Antarctic Oscillation index (AOI) outlined in Gong and Wang (1999). This index consists of the difference in normalised zonal mean sea level pressure at 40°S and 65°S. The ensemble mean AOI in the El Niño experiment is −0.1, and −0.04 in the La Niña experiment. A strong positive SAM would be indicated by an AOI of 1, but both experiments ensemble mean SAM conditions are weakly negative. Therefore there is no preference for a particular phase of SAM in either experiment. Neither is there a preferred phase of SAM for the 11 El Niño (the first 11 in Table 1) ensemble members that had fewer than the expected number of heatwave days.

This study focused on using a climate model to conduct experiments, and so comparison to other observational studies is needed in future studies to evaluate the reliability of the simulations. A key method of this study examines the role of surface heat fluxes in heatwave variability, but there are no surface flux observations for Australia that cover a long enough period to allow an analysis of ENSO conditions. The reanalysis used simulates rainfall and land surface processes, but the comparison being made is really one model with another. Nevertheless, the importance of rainfall and soil moisture in the development or suppression of heatwaves and extreme temperatures is apparent in observations (Herold et al. 2016) and in a regional climate model study (Kala et al. 2015). These studies found that the southeast regions that have low summer precipitation and soil moisture (as contrasted to the northern regions) are more strongly influenced by the synoptic climatology and climate variability modes other than ENSO. This generally agrees with our results whereby the advection of heat from lower latitudes towards southeast Australia contrasts with other northerly regions where ENSO dominates heatwave variability. The path of trajectories presented in this study is similar to previous observational studies that have examined different research questions but used similar methods. Parker et al. (2013), Boschat et al. (2014) and Quinting and Reeder (2017) demonstrate that air parcels ending at heatwaves in southeastern Australia originate over the Southern Ocean and circulate anticyclonically around the Tasman Sea. Our results demonstrate that this is true for the other eastern regions of Australia, but also that the air flows from a southeasterly direction for heatwaves in the north. It is also encouraging that other studies have found that the magnitude of the observed median diabatic heating of air approaching hot extremes is about 10 K. This is true for southeastern Australia (Fig. 10b of Quinting and Reeder 2017) and the similar latitude of central Europe (Fig. 6e of Bieli et al. 2015), both of which correspond to the 11 K in Fig. 15c.

Table 1 December–February southern annular mode index for each El Niño and La Niña ensemble member

No.	Niño	Niña	No.	Niño	Niña	No.	Niño	Niña
1	1.53	−0.26	11	0.96	0.2	21	−0.46	0.76
2	−0.22	0.74	12	−0.14	−0.58	22	0.06	−1.07
3	1.03	0.28	13	1.22	0.8	23	−0.35	−1.36
4	1.83	−0.94	14	0.42	0.11	24	−1.99	0.77
5	0.25	0.34	15	0.51	0.71	25	−1.64	−0.13
6	−1.36	−0.6	16	1.06	1.22	26	1.27	−0.69
7	−0.51	−1.56	17	0.4	1.26	27	−0.12	−0.71
8	0.2	0.14	18	−1.54	−0.18	28	−0.1	1.27
9	0.16	−0.58	19	−1.61	0.61	29	−1.84	−3.01
10	−0.27	−0.1	20	−2.33	0.35	30	0.54	0.81

The first 11 of the El Niño ensembles had fewer heatwave days in the northeast of Australia than the control simulation

While there is generally good agreement of the ACCESS model to observational studies, the Traj3d tracking scheme suffers from some of the common limitations of Lagrangian tracking schemes. For example, because of the discrete wind field and advection method, the calculated trajectory would have some error compared to a "true" path advected continuously in a real wind field. This would also make the advection non-reversible, such that back trajectories would not be identical to the forward trajectories. Furthermore, sub-grid scale process are not explicitly resolved and might have a detectable effect on heat accumulation along the trajectories. Using a high resolution regional climate model may address these problems and provide further insight into the mechanisms of heat accumulation in the atmosphere.

This study may also provide a framework for investigating how other climate variability modes might affect heatwaves. The Indian Ocean Dipole (IOD) is another mode of variability based on SST and air sea interaction that may influence heatwaves in Australia and an investigation of it may benefit from the methods used here. Other climate modes, such as the SAM and Madden–Julian Oscillation, may also interact with ENSO to produce heatwave seasons that are inconsistent with the usual impact of ENSO and should be studied further. There is also some suggestion that ENSO variants can have unique impacts on rainfall in Australia, and this may lead to differences in temperature extremes; however, Loughran et al. (2017b) have recently shown that this is unlikely for heatwaves.

In conclusion, this study has used the ACCESS climate model to simulate the heatwave response of the atmosphere to ENSO forcing, and examined how ENSO affect three heatwave development mechanisms. While the three mechanisms are all necessary for the development of a heatwave event, we have highlighted the relevance of each for different regions of Australia in the development of heatwave variability during ENSO phases. Our findings suggest that different regions of Australia are affected by ENSO in different ways, with the north and northeast being dominated by variability of land surface processes, while the east and southeast are more strongly affected by advection and subsidence of potential heat. Also, despite prevailing El Niño conditions, high soil moisture conditions may mitigate the severity of heatwaves in the north and northeastern regions. This knowledge may provide useful insights to seasonal range predictions for heatwaves, and possibly shorter duration extreme heat events. Future research might focus on the role of other climate modes in heatwave development as these may affect heatwaves in similar or contrasting ways.

Acknowledgements This work was supported and funded by the Australian Postgraduate Award, the Australian Research Councils (ARC) Discovery Early Career Researcher Award grant DE140100952, the ARC Centre of Excellence for Climate System Science Grant CE110001028 and the ARC Centre of Excellence for Climate Extremes Grant CE170100023. The modelling was undertaken with the assistance of resources provided at the NCI National Facility systems at the Australian National University through the National Computational Merit Allocation Scheme supported by the Australian Government. The HadISST data was provided the Met Office (http://www.metoffice.gov.uk/hadobs/hadisst). Thanks to Nicholas Herold at the University of New South Wales for developing the composite SST fields used to force the model. Lastly, we thank the University of Melbourne for providing access to the Traj3d Lagrangian tracking scheme.

References

Abramowitz G, Leuning R, Clark M, Pitman A (2008) Evaluating the performance of land surface models. J Clim 21(21):5468–5481. https://doi.org/10.1175/2008JCLI2378.1

Alexander L (2011) Extreme heat rooted in dry soils. Nat Geosci 4(1):12–13. https://doi.org/10.1038/ngeo1045

Arblaster JM, Alexander LV (2012) The impact of the El Nio–Southern Oscillation on maximum temperature extremes. Geophys Res Lett. https://doi.org/10.1029/2012GL053409

Arblaster JM, Lim EP, Hendon HH, Trewin BC, Wheeler MC, Liu G, Braganza K (2014) Understanding Australia's Hottest September on record. Spec Suppl Bull Am Meteorol Soc 95(9):37–41

Ashcroft L, Karoly DJ, Gergis J (2014) Southeastern Australian climate variability 1860–2009: a multivariate analysis. Int J Climatol 34(6):1928–1944. https://doi.org/10.1002/joc.3812

Barras V, Simmonds I (2009) Observation and modeling of stable water isotopes as diagnostics of rainfall dynamics over southeastern Australia. J Geophys Res Atmos. https://doi.org/10.1029/2009JD012132

Best M, Abramowitz G, Johnson H, Pitman A, Balsamo G, Boone A, Cuntz M, Decharme B, Dirmeyer P, Dong J, Ek M, Guo Z, Haverd V, van den Hurk B, Nearing G, Pak B, Peters-Lidard C, Santanello JAJ, Stevens L, Vuichard N (2015) The plumbing of land surface models: benchmarking model performance. J Hydrometeorol 16(June 2015):1425–1442. https://doi.org/10.1175/JHM-D-14-0158.1

Bi D, Dix M, Marsland SJ, Farrell SO, Rashid HA, Uotila P, Hirst AC, Kowalczyk E, Golebiewski M, Sullivan A, Yan H, Hannah N, Franklin C, Sun Z, Vohralik P, Watterson I, Zhou X, Fiedler R, Collier M, Ma Y, Noonan J, Stevens L, Uhe P, Zhu H, Griffies SM, Hill R, Harris C, Puri K (2013) The ACCESS coupled model: description, control climate and evaluation. Aust Meteorol Oceanogr J 63:41–64

Bieli M, Pfahl S, Wernli H (2015) A lagrangian investigation of hot and cold temperature extremes in Europe. Q J R Meteorol Soc 141(686):98–108. https://doi.org/10.1002/qj.2339

Boschat G, Pezza A, Simmonds I, Perkins S, Cowan T, Purich A (2014) Large scale and sub-regional connections in the lead up to summer heat wave and extreme rainfall events in eastern Australia. Clim Dyn 44:1823–1840. https://doi.org/10.1007/s00382-014-2214-5

Boschat G, Simmonds I, Purich A, Cowan T, Pezza AB (2016) On the use of composite analyses to form physical hypotheses: an example from heat wave—SST associations. Nat Publ Group (January). https://doi.org/10.1038/srep29599

Bureau of Meteorology (2016a) Annual Climate Report 2015. Bureau of Meteorology, Melbourne, p 31

Bureau of Meteorology (2016b) Special Climate Statement 53 widespread record December temperatures in southeast Australia. Bureau of Meteorology, Melbourne

Chambers CRS, Chambers CRS, Brassington GB, Simmonds I, Walsh K (2014) Precipitation changes due to the introduction of eddy-resolved sea surface temperatures into simulations of

the "Pasha Bulker" Australian east coast low of June 2007. Meteorol Atmos Phys 125:1–15. https://doi.org/10.1007/s00703-014-0318-4

Coates L (1996) An overview of fatalities from some natural hazards in Australia. In Proceedings of conference on natural disaster reduction (October), pp 49–54

Coates L, Haynes K, O'Brien J, McAneney J, De Oliveira FD (2014) Exploring 167 years of vulnerability: an examination of extreme heat events in Australia 1844–2010. Environ Sci Policy 42:33–44. https://doi.org/10.1016/j.envsci.2014.05.003

Colombo AF, Etkin D, Karney BW (1999) Climate variability and the frequency of extreme temperature events for nine sites across Canada: implications for power usage. J Clim 12(8 PART 2):2490–2502. https://doi.org/10.1175/1520-0442(1999)012h2490:CVATFOi2.0.CO;2

Compo GP, Whitaker JS, Sardeshmukh PD, Matsui N, Allan RJ, Yin X, Gleason BE, Vose RS, Rutledge G, Bessemoulin P, Br¨onnimann S, Brunet M, Crouthamel RI, Grant AN, Groisman PY, Jones PD, Kruk MC, Kruger AC, Marshall GJ, Maugeri M, Mok HY, Nordli Ø, Ross TF, Trigo RM, Wang XL, Woodruff SD, Worley SJ (2011) The twentieth century reanalysis project. Q J R Meteorol Soc 137(654):1–28. https://doi.org/10.1002/qj.776

Coumou D, Rahmstorf S (2012) A decade of weather extremes. Nat Clim Change (March). https://doi.org/10.1038/nclimate1452

Cowan T, Purich A, Perkins S, Pezza A, Boschat G, Sadler K (2014) More frequent, longer and hotter heat waves for Australia in the 21st century. J Clim 27:5851–5871. https://doi.org/10.1175/JCLI-D-14-00092.1

CRED (2015) The Human costs of weather related disasters. Centre for Research on the Epidemiology of Disasters—The United Nations Office for Diaster Risk Reduction, p 37. https://doi.org/10.1017/CBO9781107415324.004. http://arxiv.org/abs/1011.1669v3

Davies T, Cullen MJP, Malcolm AJ, Mawson MH, Staniforth A, White AA, Wood N (2005) A new dynamical core for the Met Office's global and regional modelling of the atmosphere. Q J R Meteorol Soc 131(608):1759–1782. https://doi.org/10.1256/qj.04.101

Decker WL (1967) Periods with Temperatures Critical to Agriculture. No. 864 in North central regional research publications, University of Missouri, Agricultural Experiment Station

Deser C, Knutti R, Solomon S, Phillips AS (2012) Communication of the role of natural variability in future North American climate. Nat Clim Change 2(11):775–779. https://doi.org/10.1038/nclimate1562

Farooq M, Bramley H, Palta JA, Kadambot HM, Farooq M, Bramley H, Palta JA, Siddique KHM (2016) Heat stress in wheat during reproductive and grain-filling phases. Crit Rev Plant Sci 2689(April):491–507. https://doi.org/10.1080/07352689.2011.615687

Frich P, Alexander LV, Gleason B, Haylock M, Klein Tank AMG, Peterson T (2002) Observed coherent changes in climatic extremes during the second half of the twentieth century. Clim Res 19(3):193–212

Gong D, Wang S (1999) Definition of Antarctic Oscillation Index. Geophys Res Lett 26(4):459–462. https://doi.org/10.1029/1999GL900003

Green D, Pitman A, Barnett A, Kaldor J, Doherty P, Stanley F (2017) Advancing Australia's role in climate change and health research. Nat Clim Change 7(2):103–106. https://doi.org/10.1038/nclimate3182

Harpaz T, Ziv B, Saaroni H, Beja E (2014) Extreme summer temperatures in the East Mediterranean-dynamical analysis. Int J Climatol 34(3):849–862. https://doi.org/10.1002/joc.3727

Hendon HH, Thompson DWJ, Wheeler MC (2007) Australian rainfall and surface temperature variations associated with the Southern Hemisphere annular mode. J Clim 20:2452–2467. https://doi.org/10.1175/JCLI4134.1

Herold N, Kala J, Alexander LV (2016) The influence of soil moisture deficits on australian heatwaves. Environ Res Lett 11(6):1–8. https://doi.org/10.1088/1748-9326/11/6/064003

Hirschi M, Seneviratne SI, Alexandrov V, Boberg F, Boroneant C, Christensen OB, Formayer H, Orlowsky B, Stepanek P (2010) Observational evidence for soilmoisture impact on hot extremes in southeastern Europe. Nat Geosci 4(1):17–21. https://doi.org/10.1038/ngeo1032

IPCC (2013) Climate change 2013: the physical science basis. Contribution of working group I to the fifth assessment report of the intergovernmental panel on climate change. Cambridge University Press, Cambridge. https://doi.org/10.1017/CBO9781107415324

Kala J, Evans JP, Pitman AJ (2015) Influence of antecedent soil moisture conditions on the synoptic meteorology of the black saturday bushfire event in southeast Australia. Q J R Meteorol Soc 141:3118–3129. https://doi.org/10.1002/qj.2596

Karoly DJ (1989) Southern Hemisphere circulation features associated with El Niño-Southern Oscillation events. J Clim 2(11):1239–1252. https://doi.org/10.1175/1520-442(1989)002h1239:SHCFAWi2.0.CO;2

King AD, Donat MG, Alexander LV, Karoly DJ (2015) The ENSO-Australian rainfall teleconnection in reanalysis and CMIP5. Clim Dyn 44(9–10):2623–2635. https://doi.org/10.1007/s00382-014-2159-8

Klingaman NP, Woolnough SJ, Syktus J (2013) On the drivers of interannual and decadal rainfall variability in Queensland, Australia. Int J Climatol 33(10):2413–2430. https://doi.org/10.1002/joc.3593

Kowalczyk EA, Stevens L, Law RM, Dix M, Wang YP, Harman IN, Haynes K, Srbinovsky J, Pak B, Ziehn T (2013) The land surface model component of ACCESS: description and impact on the simulated surface climatology. Aust Meteorol Oceanogr J 63:65–82

L'Heureux ML, Thompson DWJ (2006) Observed relationships between the El-Niño–Southern oscillation and the extratropical zonal-mean circulation. J Clim 19(1):276–287. https://doi.org/10.1175/JCLI3617.1

Lim EP, Hendon HH (2015) Understanding the contrast of Australian springtime rainfall of 1997 and 2002 in the frame of two flavors of El Niño. J Clim 28(7):2804–2822. https://doi.org/10.1175/JCLI-D-14-00582.1

Lorenz R, Jaeger EB, Seneviratne SI (2010) Persistence of heat waves and its link to soil moisture memory. Geophys Res Lett 37(9):1–5. https://doi.org/10.1029/2010GL042764

Loughran TF, Perkins-Kirkpatrick SE, Alexander LV (2017a) Understanding the spatio-temporal influence of climate variability on Australian heatwaves. Int J Climatol 37(10):3963–3975. https://doi.org/10.1002/joc.4971

Loughran TF, Perkins-Kirkpatrick SE, Alexander LV, Pitman AJ (2017b) No significant difference between Australian heatwave impacts of Modoki and Eastern Pacific El Niño. Geophys Res Lett 44:5150–5157. https://doi.org/10.1002/2017GL073231

Marshall AG, Hudson D, Wheeler MC, Hendon HH, Alves O (2012) Simulation and prediction of the Southern annular mode and its influence on Australian intra-seasonal climate in POAMA. Clim Dyn 38(11–12):2483–2502. https://doi.org/10.1007/s00382-011-1140-z

Marshall AG, Hudson D, Wheeler MC, Alves O, Hendon HH, Pook MJ, Risbey JS (2013) Intra-seasonal drivers of extreme heat over Australia in observations and POAMA-2. Clim Dyn 43:1915–1937. https://doi.org/10.1007/s00382-013-2016-1

McBride JL, Mills GA, Wain AG (2009) The Meteorology of Australian heatwaves. Modelling and understanding high impact weather: extended abstracts of the third CAWCR modelling workshop, pp 91–94

McEvoy D, Ahmed I, Mullett J (2012) The impact of the 2009 heat wave on Melbourne's critical infrastructure. Local Environ 17(8):783–796. https://doi.org/10.1080/13549839.2012.678320

Meehl GA, Tebaldi C (2004) More intense, more frequent, and longer lasting heat waves in the 21st century. Science 305(5686):994–997. https://doi.org/10.1126/science.1098704

Miralles DG, Van Den Berg MJ, Teuling AJ, De Jeu RAM (2012) Soil moisture temperature coupling: a multiscale observational analysis. Geophys Res Lett 39(21):2–7. https://doi.org/10.1029/2012GL053703

Miralles DG, Teuling AJ, Heerwaarden CCV (2014) Mega-heatwave temperatures due to combined soil desiccation and atmospheric heat accumulation. Nat Geosci 7(5):345–349. https://doi.org/10.1038/ngeo2141

Nairn J, Fawcett R, Ray D (2009) Defining and predicting excessive heat events, a national system. CAWCR Tech Rep 60:83–86

Nicholls N, Drosdowsky W, Lavery B (1997) Australian rainfall variability and change. Bur Meteorol 52(3):66–72. https://doi.org/10.1002/j.1477-8696.1997.tb06274.x

Nicholls N, Baek HJ, Gosai A, Chambers LE, Choi Y, Collins D, Della-Marta PM, Griffiths GM, Haylock MR, Iga N, Lata R, Maitrepierre L, Manton MJ, Nakamigawa H, Ouprasitwong N, Solofa D, Tahani L, Thuy DT, Tibig L, Trewin B, Vediapan K, Zhai P (2005) The El Niñno-Southern Oscillation and daily temperature extremes in east Asia and the west Pacific. Geophys Res Lett 32(16):1–4. https://doi.org/10.1029/2005GL022621

Noone D, Simmonds I (1999) A three-dimensional spherical trajectory algorithm. Res Activities Atmos Ocean Model 28(942):3.26–3.27

Parker TJ, Berry GJ, Reeder MJ (2013) The influence of tropical cyclones on heat waves in Southeastern Australia. Geophys Res Lett 40(23):6264–6270. https://doi.org/10.1002/2013GL058257

Parker TJ, Berry GJ, Reeder MJ (2014a) The structure and evolution of heat waves in Southeastern Australia. J Clim 27:5768–5785

Parker TJ, Berry GJ, Reeder MJ, Nicholls N (2014b) Modes of climate variability and heat waves in Victoria, southeastern Australia. Geophys Res Lett 41(19):6926–6934. https://doi.org/10.1002/2014GL061736

Pepler AS, Alexander LV, Evans JP, Sherwood SC (2016) The influence of local sea surface temperatures on Australian east coast cyclones. J Geophys Res 121:13352–13363. https://doi.org/10.1002/2016JD025495

Perkins SE (2015) A review on the scientific understanding of heatwaves—their measurement, driving mechanisms, and changes at the global scale. Atmos Res 164:242–267. https://doi.org/10.1016/j.atmosres.2015.05.014

Perkins SE, Alexander LV (2013) On the measurement of heat waves. J Clim 26(13):4500–4517. https://doi.org/10.1175/JCLI-D-12-00383.1

Perkins SE, Alexander LV, Nairn JR (2012) Increasing frequency, intensity and duration of observed global heatwaves and warm spells. Geophys Res Lett. https://doi.org/10.1029/2012GL053361

Perkins SE, Argüeso D, White CJ (2015) Relationships between climate variability, soil moisture, and Australian heatwaves. J Geophys Res Atmos 120(16):8144–8164. https://doi.org/10.1002/2015JD023592

Pezza AB, Rensch P, Cai W (2012) Severe heat waves in Southern Australia: synoptic climatology and large scale connections. Clim Dyn 38(1–2):209–224. https://doi.org/10.1007/s00382-011-1016-2

Quinting JF, Reeder MJ (2017) Southeastern Australian heat waves from a trajectory viewpoint. Mon Weather Rev 145(10):4109–4125. https://doi.org/10.1175/MWR-D-17-0165.1

Rasmusson EM, Carpenter TH (1982) Variations in tropical sea surface temperature and surface wind fields associated with the southern oscillation/El Niño. Mon Weather Rev 110:354–384

Rayner NA (2003) Global analyses of sea surface temperature, sea ice, and night marine air temperature since the late nineteenth century. J Geophys Res 108(D14):4407. https://doi.org/10.1029/2002JD002670

Risbey JS, Pook MJ, McIntosh PC, Wheeler MC, Hendon HH (2009) On the remote drivers of rainfall variability in Australia. Mon Weather Rev 137(10):3233–3253. https://doi.org/10.1175/2009MWR2861.1

Seager R, Harnik N, Kushnir Y, Robinson WA, Miller JA (2003) Mechanisms of hemispherically symetric climate variability. J Clim 16(18):2960–2978. https://doi.org/10.1175/1520-0442(2003)016h2960:MOHSCVi2.0.CO;2

Seneviratne SI, Corti T, Davin EL, Hirschi M, Jaeger EB, Lehner I, Orlowsky B, Teuling AJ (2010) Investigating soil moisture–climate interactions in a changing climate: a review. Earth Sci Rev 99(3–4):125–161. https://doi.org/10.1016/j.earscirev.2010.02.004

Trenberth KE (1976) Spatial and temporal variations of the Southern Oscillation. Q J R Meteorol Soc 102(433):639–653. https://doi.org/10.1002/qj.49710243310

Victorian Department of Health (2009) January 2009 heatwave in Victoria: an assessment of health impacts (January). Victorian Government Deparment of Human Services, Melbourne, Victoria, p 24. https://www2.health.vic.gov.au/Api/downloadmedia/%7B959CCD3C-8285-4938-872E-62E15AA62C62%7D

Wang YP, Kowalczyk E, Leuning R, Abramowitz G, Raupach MR, Pak B, Van Gorsel E, Luhar A (2011) Diagnosing errors in a land surface model (CABLE) in the time and frequency domains. J Geophys Res Biogeosci 116(1):1–19. https://doi.org/10.1029/2010JG001385

Welbergen JA, Klose SM, Markus N, Eby P (2008) Climate change and the effects of temperature extremes on Australian flying-foxes. Proc R Soc B Biol Sci 275(1633):419–425. https://doi.org/10.1098/rspb.2007.1385

World Meteorological Organisation (2016) Provisional WMO statement on the status of the global climate in 2016 (1189). World Meteorological Organisation, Geneva, Switzerland. ISBN 97892631111890. https://public.wmo.int/en/media/press-release/provisional-wmo-statement-status-of-global-climate-2016

Zander KK, Botzen WJW, Oppermann E, Kjellstrom T, Garnett ST (2015) Heat stress causes substantial labour productivity loss in Australia. Nat Clim Change 5(May):1–6. https://doi.org/10.1038/nclimate2623

Zhang H, Pak B, Wang YP, Zhou X, Zhang Y, Zhang L (2013) Evaluating surface water cycle simulated by the Australian community land surface model (CABLE) across different spatial and temporal domains. J Hydrometeorol 14(4):1119–1138. https://doi.org/10.1175/JHM-D-12-0123.1